ECSS 2007 Abstracts by session

ECSS 2007 - 4th European Conference on Severe Storms, Trieste, Italy, 10-14 September 2007
List of the abstract accepted for presentation at the conference:
O - Oral presentation
P - Poster presentation

I. SECTION: 05 - (LOU BATTAN SESSION) SEVERE STORMS AND RADAR INFORMATION

Sec.N	Type	Abstract Title	Author(s)
05.01	**O**	*Weather Radar - Forthcoming technology and issues that it might resolve*	Zrnic Dusan
05.02	**O**	*Mobile Doppler RADAR observations of tornadoes*	Bluestein Howard
05.03	**O**	*Analysis of a tornadic mini-supercell in Finland by using Doppler RADAR*	Teittinen Jenni
05.04	**O**	*Nowcasting severe storms in the central area of the State of Sao Paulo with the aid of TITAN*	Held Ana Maria Held Gerhard
05.05	**O**	*Polarimetric Doppler RADAR analysis of the 3rd August 2006 supercell storm*	Alberoni Pier Paolo
05.06	**O**	*UHF RADAR studies of vertical motion and turbulence characteristics in the pre-monsoon thunderstorm over an Indian tropical station*	Deshpande Sachin Madhukar
05.07	**O**	*Windfield reconstruction over convective storms by using along-track technique*	Alberoni Pier Paolo Goh Yong Kheng
05.08	**O**	*Detection of turbulence generated by convective motion by an X-band Doppler RADAR: the DTCOR method*	kemkemian stephane
05.09	**O**	*Signature of severe thunderstorms for nowcasting in the state of Sao Paulo, Brazil*	Held Ana Maria Held Gerhard
05.10	P	*Hail cells features and probability of hail equations in the region of Ebro valley*	Ceperuelo Manuel Tomeu Rigo
05.11	P	*Quantitative precipitation forecast using RADAR echo extapolation*	Novak Petr Salek Milan
05.12	P	*Investigation of large vertical depth Cb in India*	Sinkevich Andrey Alexandrovich
05.13	P	*The European weather RADAR network (OPERA)*	Delobbe Laurent
05.14	P	*Case study of a Tornadic supercell in Finland 28th August 2005*	outinen kaisa Teittinen Jenni
05.15	P	*Study on the mesoscale structure of heavy rainfall on Meiyu front with dual-Doppler RADAR*	zhou haiguang
05.16	P	*Rain event on 22 October 2006 in Leon (Spain): drop size spectra*	Fraile Roberto Palencia Covadonga
05.17	P	*Discriminant analysis applied onto hail detection using RADAR*	Garcia-Ortega Eduardo LOPEZ LAURA
05.18	P	*Characterization of convective rainfall using C-band dual-polarized RADAR and Models intercomparison: COSMO-LAMI and MM5*	Ferretti Rossella

II. SECTION: 05 - (LOU BATTAN SESSION) SEVERE STORMS AND RADAR INFORMATION (CONT'D)

Sec.N	Type	Abstract Title	Author(s)
05.19	P	*The statistical characteristics of results of RADAR observations of atmospheric phenomena related to Cb*	Huseynov Nazim Malikov Bahruz
05.20	P	*Seasonal and interannual variations of Indian summer monsoon winds - a study using Indian MST RADAR*	Mekalathur RAMAN ROJA
05.21	P	*Observing and analysing mesoscale vortices by weather RADAR*	Zhu Xiaoyan
05.22	P	*RADAR tracking method for cloud seeding experimental units over Cuba*	novo sadiel novo
05.23	P	*Simulations of X-band thunderstorms RADAR observations*	Pujol Olivier
05.24	P	*An Evaluation of ECMWF Analyses Sounding Parameters in Thunderstorm and Severe Local Storm Forecasting for Europe.*	Dotzek Nikolai kaltenboeck rudolf
05.25	P	*Measurements for extreme rainfall estimation: comparison with estimates based on horizontal reflectivity*	bechini renzo

WEATHER RADAR
FORTHCOMING TECHNOLOGY AND ISSUES IT MIGHT RESOLVE

Dusan Zrnic

National Sever Storms Laboratory, 120 David Boren Blvd, Norman OK 73072, USA, dusan.zrnic@noaa.gov

(Dated: September 12, 2007)

I. INTRODUCTION

Radar meteorology was born in mid twentieth century and matured to a point that many national weather serviced routinely operate conventional radars for measuring precipitation and issuing warnings about storm severity. Doppler radars are a product of scientific and technologic advances in the later part of the century. Applications range from gauging storm severity, detecting tornadoes and measuring wind shear, to assimilating wind data into numerical weather prediction models.

What novelty is left for radar meteorologists and engineers one might ask in view of such proliferation and improvement in the radar systems? For one, there is polarization diversity, the last major advance made at the end of the century; in this discipline much scientific discovery remains. The National Weather Service of the USA plans to upgrade its network of Doppler radars to dual polarization starting in about 2009.

In the cited advances a couple of issues were secondary and hence not addressed. One is the speed of volume coverage. Although phased array radars for tactical applications have been around for some thirty years, exploration of their potential in the weather arena begun very recently. Two is the omnipresent radar problem of increased transverse width of the resolution volume and height above ground even at modest range; it can not be solved with single radar. These two needs, speed of volume coverage and observation close to ground are being addressed in the USA

II. ISSUES

Herein I discuss some problems and issues that might be resolved with polarimetric radars, fast scan radars, and a dense network of small radars.

Discrimination of precipitation types and determination of water accumulation is a long standing problem. Conventional and Doppler radars are contributing much to its solution. But, even if pushed to the limits of sophistication, there will remain situations for which single polarized radars fall short from providing satisfactory estimates of amounts and types of precipitation. This is, for example, because hail size and presence is inferred from indirect measurements of storm structure, and problems of rainfall estimation are inherent to methods that use backscattered power. Recent breakthroughs in radar polarimetry have been made that address these deficiencies.

The crux is to clearly separate meteorological contributions to radar returns from non meteorological ones. That step is followed by classification of precipitation type after which quantitative relations between polarimetric variables amounts of each type are invoked. Further help comes from the capability to identify directly from radar observations the location of the melting layer. Examples of these successes will be presented.

Accurate forecast of hail storms and gauging hail size remains an acute problem. Polarimetry offers some possibilities. Low values of correlation coefficient between horizontally (H) and vertically (V) polarized waves have been associated with hail. It is hypothesized that large hail can be foretold from negative values of differential reflectivity and a combination of reflectivity and differential reflectivity. Examples of success and its limitation will be presented.

Precise cause of tornado formation is not well understood. Lately clues have been sought in the inflow outflow region within few hundred meters above ground in supercell thunderstorms. How to measure the flow at these levels at such early stages is not obvious. It is accepted that cutoff of the inflow by outflow that is too strong cuts the storm life and thus might kill the tornado too. The role of precipitation is being investigated with models and data. Some hints of microphysical processes occurring in the lowest levels of supercell storms have been obtained from conceptual model of size sorting in a sheared flow. These will be presented. Detection of tornado touch down is possible in the signatures of differential reflectivity and correlation coefficient. Hence the demise is also obvious. Still finding precursors is elusive.

There are at least three desirable features that can not be achieved with the current Doppler and/or polarimetric technology. These are a) update of volume scans at intervals of 1 minute or less, b) observations near ground over large areas, and c) multipurpose use to sample weather, control air traffic, and track non cooperative airplanes. The agile beam phased array technology can deal with issues a) and c) whereas a dense network of small, short wavelength radars is a contender to alleviate b). Although rapid scans near ground do not guarantee success in understanding tornado genesis they certainly will increase warning time. Earlier detection of impending microbursts and macrobursts is also expected.

Combined with polarimetric capability rapid scan radar is the ultimate in radar meteorology. It should offer benefits in precipitation classification, in quantitative measurements, and in observations of rapidly evolving phenomena. It might even be possible to predict initiation of lightning. An example of lightning locations and successions of rapidly obtained radar reflectivity fields hint to such possibilities. Whereas the benefits are obvious for understanding the storm engine and for nowcasting applications it is not known how to incorporate these measurements into numerical weather prediction models. Challenges are: data void regions, need for better parametization (possibly with help of polarimetric measurements), and assimilation of rapid polarimetric data into the models.

ANALYSIS OF A TORNADIC MINI-SUPERCELL IN FINLAND BY USING DOPPLER RADAR

Jenni Teittinen[1], James G. LaDue[2], Harri Hohti[1] and Rodger A. Brown[3]

[1]*Finnish Meteorological Institute, Finland, jenni.teittinen@fmi.fi*

[2]*NOAA, NWS Warning Decision Training Branch, USA*

[3]*NOAA, National Severe Storms Laboratory, USA*

(Dated: 30 April 2007)

I. INTRODUCTION

In the afternoon of 18 August 2004, a tornado developed with a supercell thunderstorm in southern Finland only 17 km from the Anjalankoski Doppler radar. Based on a ground survey the tornado caused a 2.3 km long damage path damaging several buildings and blowing down trees. The cyclonic vortex caused F1 damage. No severe storm or tornado warning was issued.

The objective of this study is to try to understand why a tornado developed within this particular storm in an environment which is not known to favor tornadogenesis. A particular interest is to find out what kind of severe storm and tornado radar signatures the storm had before tornado formation to help the future warning process.

II. THE STORM ENVIRONMENT

During 18 August an occluded low over Finland was weakening and moving northeast. The warm and humid air mass stretched from south to Baltic Countries and to southern coast of Finland. Cold advection in western Finland forced the occlusion front of the cyclone to bend back and move southeast. Strong near-surface convergence along the southeast-moving bent-back occlusion initiated the tornado-producing storm. South of the front winds were from southwest and on its northern side from north or northwest.

At the tornado location (based on Anjalankoski radar measurements), the wind profile was characterized by south to southwest winds at surface, veering of the wind in lowest 5000 meters to westerly and backing of the wind above. Deep layer shear was growing as the westerly upper level jet intensified over the area (see figure 1). The 0-6 km shear of 22 m/s was adequate for supercells (Weisman 1996), however the 0-1 km shear of 7 m/s was weaker than typically associated with significant tornadoes (Markowski et al. 2003). It is important to note that many significant tornadoes have been documented with 0-1 km shear values equal to or less than found here. It is possible that the supercell encountered higher 0-1 km shear values as it encountered an outflow boundary from the south. Two other storms with mini-supercell features also developed along the surface boundary. No severe weather was observed within these storms.

III. RADAR ANALYSIS

The parent storm started as a northeastward propagating multicell storm transforming into a supercell as an outflow boundary of a nearby storm reached it from the south. The supercell turned to the right of the mean wind at approximately 30 km/h. The storm evolution is visualized in the time-height profile of the maximum reflectivity of the storm at 1130-1400 UTC (Fig. 2). The profile shows contours ascending in time at 1145-1250 UTC indicating updraft growth. Prior to tornado formation the storm echo top increases in height to its maximum. Reflectivity increases over time above the freezing level indicating hail or graupel growing in size. After the tornado at 1300-1400 UTC, the reflectivity maximum reaching the ground suggests possibly heavy rain, hail or graupel or strong outflow winds at the surface (Brown and Torgerson 2003). Within this storm, hail was not reported.

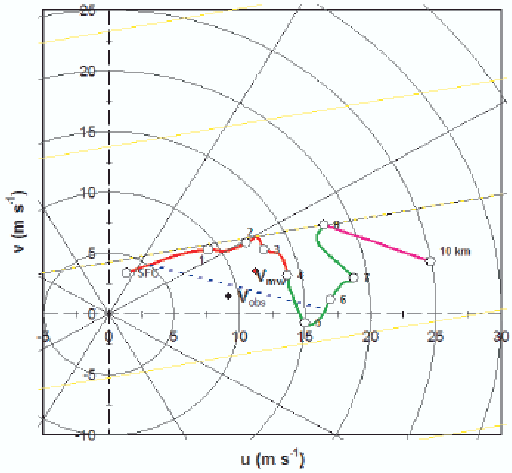

FIG. 1: A hodograph derived from a velocity wind profile derived from the Anjalankoski radar at 1245 UTC just to the north of the supercell track. The observed storm motion is plotted as $\mathbf{V_{obs}}$, $\mathbf{V_{mw}}$ is the mean 0-6 km wind.

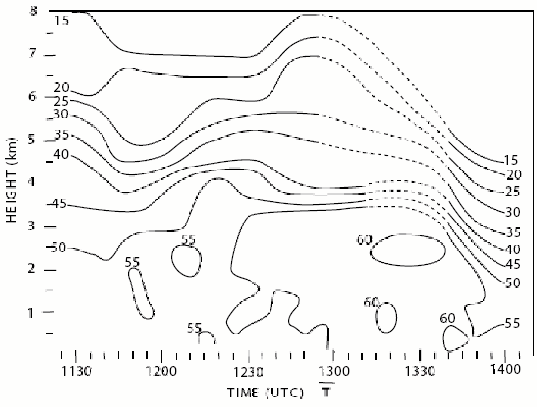

FIG. 2: Time-height representations of data for the storm on 18 August 2004, with contours of reflectivity dBZ. Tornado time (denoted by T) is 1255-1300 UTC. Dashed line is the assumed isolines when the storm is close to the radar.

The supercell thunderstorm produced a distinct hook echo during (Fig. 3) and up to 45 minutes prior to tornadogenesis. A Bounded Weak Echo Region, BWER, became visible by radar during the storm's tornadic phase. The tornado was situated in the tip of the hook. The diameter of the storm defined by 15 dBZ reflectivity contour was 20 km and the cloud top generally below 8 km. While the echo top was initially above the strongest reflectivity gradient above the storm main core, it moved over the bounded weak echo region during the time of the tornado. A shifting of an echo top toward the updraft flank is an indication of a storm becoming severe (Lemon 1980).

Overall, the Doppler velocity data showed a mesocyclone signature associated with the hook echo. The mesocyclone was convergent at the 400-500 m height and was successively less convergent with increasing height indicating that the mesocyclone was coincident with an updraft. The presence of tornadic vortex signature (TVS) appears to have biased the apparent parent mesocyclone circulation center. The observed velocity pattern resembles the simulated Doppler velocity pattern of Brown and Wood (1991) in a case where the TVS peak tangential velocity is 2 times that of a convergent mesocyclone and the location of the TVS center is closer to the edge of the mesocyclone core region. A divergence pattern behind the TVS was observed, which appears to be a rear-flank downdraft (RFD).

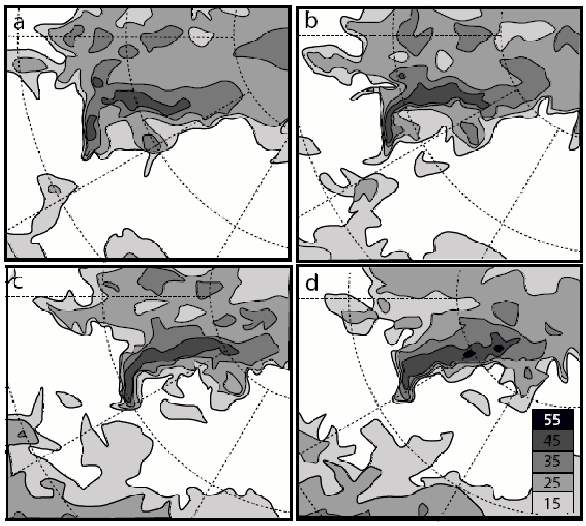

FIG. 3: PPI of reflectivity at 0.3˚ elevation at a) 1245 b) 1250 c) 1255 d) 1300 UTC. The tornado is at ground 1255-1300 UTC.

Ten minutes before the first tornado report the Doppler velocity pattern showed a mesocyclone signature which had stronger circulation maximum close to ground. At the 1.3 km height, the mesocyclone core diameter was 3.5 km. A TVS had already descended to the ground, which is pronounced at the 0.9 and 1.3 km height, where there was strong divergence close to the TVS and behind (right of) the tip of the hook. At 1.7 and 1.2 km height, 5 minutes later, weak anticyclonic rotation in the divergence area at the tip of the hook was observed (Fig. 4a). At the tornado time, 1255 UTC, the TVS tilts in height towards the mesocyclone center (Fig. 4b and 4d). At the 400 m height the TVS is situated at the tornado starting point and shows pure cyclonic rotation (Fig. 4d), while at 1.0 km height the rotation is divergent (Fig. 4b). At the tornado dissipation time at 1300 UTC (not shown) the TVS is still apparent at 900 m height but the rotation (with center over the end point of the tornado damage track) weakened considerably closer to the ground.

Within the mesocyclone, the measured peak tangential velocities were ± 11 m/s. Although the tornado was weak in strength and its diameter was less than 200 meters at the ground, the radar measured maximum Doppler velocity difference within the TVS of 20 m/s. This value is less than the mean maximum differential velocity of 36 m/s observed with tornadic TVSs in the United States (Marzban 2002). The TVS underestimates the tornado peak tangential velocity and overestimates its radius owing to the small vortex within a larger sample volume (Brown and Wood 1991). Both mesocyclone signature and TVS had spatial and temporal continuity for at least four 5-minute time steps and three elevation angles before and during the tornado.

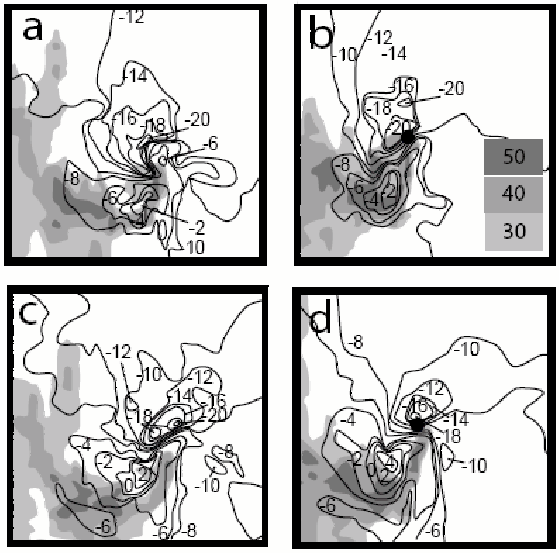

FIG. 4: B-scan picture of Doppler velocity (contours) a) 1250 UTC at 2.7˚ b) 1255 UTC at 2.7˚ c) 1250 UTC at 0.8˚ and d) 1255 UTC at 0.8˚ elevation. The shaded area is the radar reflectivity in dBZ. The radar is situated to the left of each panel with azimuth increasing from 210˚ at top of panel to 270˚ at bottom. Range increases along the bottom of each panel from 5 to 35 km from the radar. The tornado damage path starting point is denoted in 1255 UTC pictures (b and d) by a black circle.

IV. REFERENCES

Brown, R. A., Torgerson K. L., 2003: Interpretation of single-Doppler radar signatures in a V-shaped hailstorm: Part I - Evolution of reflectivity-based features. *National Weather Digest*, 27, 3-14.

Brown, R. A., Wood V. T., 1991: On the interpretation of single-Doppler velocity patterns within severe thunderstorms. *Wea. Forecasting*, 6, 32-48.

Lemon, L. R., 1980: Severe thunderstorm radar identification techniques and warning criteria: A preliminary report. NOAA Tech. Memo. NWS NSSFC-1. 60 pp. [NTIS PB273049.]

Markowski, P., Hannon C., Frame J., Lancaster E., Pietrycha A., Edwards R., Thompson R. L., 2003: Characteristics of vertical wind profiles near supercells obtained from the Rapid Update Cycle, *Wea. Forecasting*, 6, 1262-1272.

Marzban, C., 2002: Tornado Warning Guidance based on analysis of MDA/TDA/NSE data. [Available online at: http://www.wdtb.noaa.gov/modules/twg02/twg2001stats.pdf].

Teittinen J., 2002: Case studies of three tornadoes in Finland, Preprints, *European Conference on Severe Storms*, Prague, 32.

Weisman, M. L., 1996: On the use of vertical wind shear versus helicity in interpreting supercell dynamics. Preprints, *18th Conf. on Severe Local Storms*. San Francisco, CA, Amer. Meteor. Soc., 200-204.

NOWCASTING SEVERE STORMS IN THE CENTRAL AREA OF THE STATE OF SÃO PAULO WITH THE AID OF TITAN

Ana Maria Gomes and Gerhard Held

Instituto de Pesquisas Meteorológicas, Universidade Estadual Paulista, Bauru, S.P., Brazil
ana@ipmet.unesp.br; gerhard@ipmet.unesp.br
(Dated: September 12, 2007)

I. INTRODUCTION

Until recently very little was available at IPMet to be deployed as a nowcasting tool, once there was no automatic procedure for detecting and tracking potentially severe cells and to forecast their evolution and displacement. Through a collaborative effort with scientists from the National Center for Atmospheric Research (NCAR), the software system **TITAN** (**T**hunderstorm **I**dentification, **T**racking, **A**nalysis and **N**owcasting; Dixon and Wiener, 1993) was made available to analyze radar data information from both radars operated by IPMet. The implementation in IPMet´s computer system was done with the assistance of NCAR staff that helped with all necessary computer routines to be adapted for direct access to the data format generated by both Doppler radars (Kokitsu, 2005). The results that will be presented here are part of the project validation of the severe events in the central area of the State of São Paulo in compliance with some objectives of the SIHESP (Sistema Hidrometeorológico do Estado de São Paulo) project.

The main objective of the study is to verify the potential of the new tools available with the TITAN system and then to transfer the results to the operational sector of IPMet. Results related to a severe event that occurred on 17 October 1999, causing extensive damage by hail, will be presented as an example.

II. DATA AND METHODOLOGY

The Doppler radars are located at Bauru (Lat: 22.36°S, Lon: 49.02°W, 624 m amsl) and 240 km further west at Presidente Prudente (Figure 1). The main characteristics of the radar are: 2° beam width and ranges of 450 km for surveillance and 240 km in volume scan mode (11 elevations: 0.3° to 34.9°), 1 km radial and 1° azimuthal resolution, and temporal resolution of 15 min or less, recording reflectivity, radial velocity and spectral width.

TITAN was used in the *ARCHIVE* mode and the tracking properties form the base for the analysis here. A TITAN cell was defined by the 40 dBZ threshold for the reflectivity with a minimum volume of 50 km^3, observed at least in two volume scans (15 minutes). For all storms complying with or exceeding the adopted criteria for storm properties, the hail metrics, as well as the forecasting of its evolution, were determined.

Severe Storm Parameter Indicator

Besides tracking and nowcasting the movement of storm cells, TITAN has incorporated algorithms that allow identification of potentially severe storm "signatures", such as hail metrics, to produce probability of hail (POH), based on Waldvogel *et al.* (1979). This implies that hail occurs always when the 45 dBZ reflectivity is present at 1.4 km or more above the freezing level. Another parameter, FOKR (Foote-Kraus) index, also related to hail-producing storms, was developed by Foote *et al.* (2005) and first applied to hail-producing storms in Argentina. Also used for the analysis here is the SSS (Storm Structure Severity) index, developed by Visser (2001) for hailstorms on the South African Plateau.

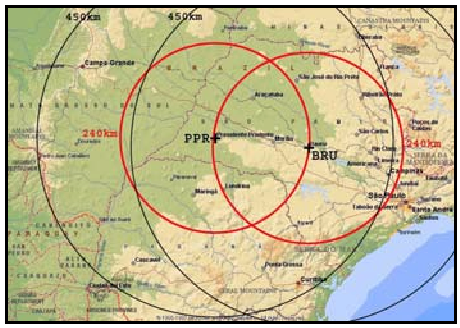

FIG. 1: Doppler radar network of IPMet (BRU = Bauru; PPR = Presidente Prudente), showing range rings for 240 and 450 km.

III. DISCUSSION AND RESULTS

Storm Overview

The severe event on 17 October 1999 developed and evolved in an environment under the influence of a baroclinic system reaching the State of São Paulo. A squall line with multicellular storm characteristics, showing several intense cells forming ahead of the frontal disturbance, with an extended trailing stratiform area, can be seen in Figure 2.

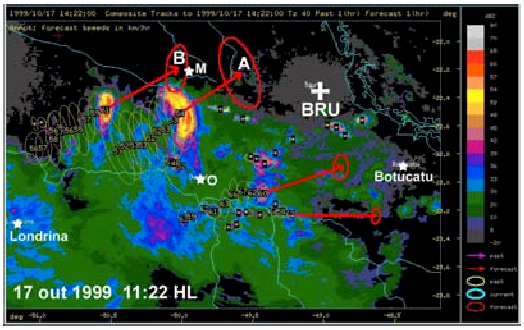

FIG 2: Composite reflectivity field for the Bauru and Presidente Prudente radars, 240 km range, on 17/10/1999, 11:22 LT. The ellipses show the areas in excess of 40 dBZ identified and tracked by TITAN (yellow: past history of the storm; blue: present; red: nowcasting for the next 60 minutes).

Hail Event of 17 October 1999

The most intense cell, labeled A, located south of Marilia (M) at 11:22 LT, is shown in Figure 2 with its trajectory and forecast for the next 60 minutes, highlighting the areas with reflectivities in excess of 40 dBZ. The cell A, that produced the hailstorm had an average speed of 60 to 65 km.h^{-1}, with reflectivities in excess of 60 dBZ, reaching a

maximum of between 70 and 72 dBZ and echo top height (10 dBZ) of 13 to 17 km, showing a very intense vertical development. Vertical cross-sections parallel to the direction of movement confirm the existence of tilted updrafts, that sustain and maintain the high reflectivities observed during the lifetime of storm A, with hail falling out at the leading edge of the storm. The storm reached areas north of Bauru, producing severe damage by hail and strong winds at around 13:00 LT.

The temporal evolution of the hail severity parameters for cell A can be seen in Figure 3, with the observations covering 30 minutes before and 30 minutes after the observed hail fall, from 12:30 to 13:30 LT. The temporal evolution for variations of the indices relating to hail metrics, such as VIHM (hail from VIL max), probability of hail (POH) and the FOKR index are shown in Figure 3. The index POH, related to the probability of hail reaching the ground, shows values very close to and even reaching 100%, from 12:37 LT to 12:59 LT. At 12:30 LT, the FOKR index reaches a number 4 category, in a classification that spans from 0 to 4, persisting until 13:15 LT, when a slight decrease in value can be seen, but still showing category 3 and 4 during the continuous movement of the storm towards the northeast sector. According to the classification by Abshaev (Foote *et al.*, 2005), the categories 0 and 1 are considered non-hail producing storms, while category 3 and 4 are hail producing storms, and the category 4 can produce 5 to 6 times more damage on the ground than category 3. The SSS index (not shown here) also exhibits a severe volume and top structure classification, with magnitudes for the index of 8 and 9, indicative of the presence of intense updrafts, important and needed for the formation and maintenance of the hail that was observed later on at the surface.

Storm Cell Tracking and Forecasting Verification

The TITAN system has a statistical module to allow the verification of the storm cell tracking and forecasting. The forecasting results can be evaluated using the performance indices, such as the Critical Success Index (CSI), which varies from 0 to 1, being desirable to have values close to 1, once this index is defined as a function of the probability of detection (POD) and of the false alarm rate (FAR). The results for the evaluation of the 17/10/1999 event are summarized in Figure 4, considering forecasting times of 15, 30, 45 and 60 minutes. The values for the probability of detection and movement of the storm cell exceeding the 40 dBZ threshold and life span greater than 15 minutes are around 70 to 74 %, having a false alarm rate of 46 to 56%. The CSI varies from 38 to 55%, for a forecasting period of 60 and 15 min, respectively. Considering the period of 30 minutes for issuing an alert for a severe storm, the performance of the forecast, represented by the CSI index, is around 45%, with the capacity for the identification and tracking by TITAN being in excess of 70%, considering the threshold adopted here.

IV. CONCLUSION

A new forecasting tool especially developed for direct application in nowcasting and implemented at IPMet was applied here for the analysis and evaluation of a severe event that occurred in the central State of São Paulo. The results produced by this preliminary analysis have demonstrated the potential use of TITAN severity indices to support the issuing of severe weather warnings within the 240 km range of the two Doppler radars operated by IPMet. The analysis will be extended to include more cases and to improve the radar bulletins issued routinely for the public in general and the local Civil Defense Authorities in particular.

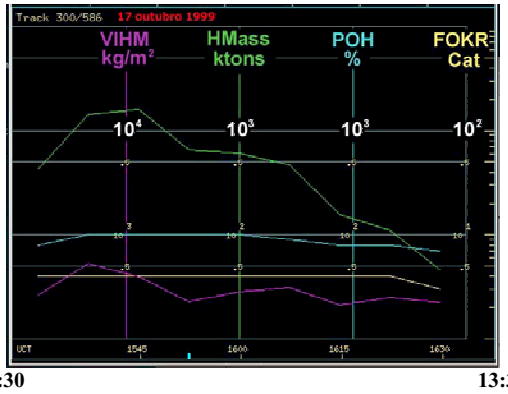

FIG 3: Temporal evolution of TITAN severity indices (POH, FOKR, etc) from the hail-producing cell observed on 17/10/99.

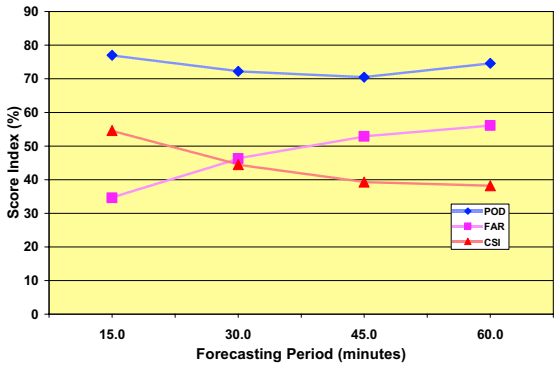

FIG. 4: Evaluation indices for the performance of the storm cell forecasting observed by the Bauru Doppler radar on 17/10/1999.

V. ACKNOWLEDGMENTS

The authors would like to thank J. M. Kokitsu for the implementation of the TITAN routines used in the analysis and HAG França for retrieving the radar data, Drs J. Wilson and M. Dixon of NCAR for facilitating the implementation of TITAN at IPMet/UNESP. FAPESP provided financial support for the upgrading of both Doppler radars – Project no. 05/54944-3 and Project SIHESP no. 01/14095-6.

VI. REFERENCES

Dixon M. and Wiener G., 1993: TITAN: Thunderstorm Identification, Tracking, Analysis and Nowcasting - A radar-based methodology. *J. Atmos. Ocean. Techn.*, **10**, 785-797.

Foote G.B., Krauss T.W. and Makitov V., 2005: Hail metrics using conventional radar. *Proc., 16th Conference on Planned and Inadvertent Weather Modification,* Jan. 2005, AMS, Boston.
In:www.ams.confex.com/ams/pdfpapers/86773.pdf .

Kokitsu J.M., 2005: *Transferência de Tecnologias para Aplicação direta ao Monitoramento e Nowcasting Usando os Radares Meteorológicos Doppler do IPMet-UNESP*. Relatório Técnico (Bolsa de Participação em Curso ou Estagio Técnico no Exterior, Período: 01/09/2005 a 01/10/2005), FAPESP Processo No. 05/54944-3, 55pp.

Visser P.J.M., 2001: The Storm-Structure-Severity method for the identification of convective storm characteristics with conventional weather radar. *Meteor. Applications,* **8**, 1-10.

Waldvogel A., Federer B. and Grimm P., 1979: Criteria for the Detection of Hail Cells, *J. Appl. Meteor.*, **18**, 1521-1525.

POLARIMETRIC DOPPLER RADAR ANALYSIS OF THE 3 AUGUST 2006 SUPERCELL STORM .

M. Celano[1], A. Fornasiero[1], P.Mezzasalma[1], F.Grazzini[1], P.P. Alberoni[1,2]

[1]*ARPA-SIM, Bologna Italy. mcelano@arpa.emr.it*
[2]*ISAC-CNR, Bologna Italy.*

I. INTRODUCTION

On 3rd August 20065 a Supercell storm sweep over the eastern part of the Po Valley, this study present an analysis on the case using the ARPA-SIM polarimetric C-band radar network.

It is well known that radar reflectivity measures are affected by a wide spectrum of error sources. Their variable effect in time and space is the major limitation to the systematic use of radar informations in the description of severe storms. The correction procedures implemented commonly in the systems managing radar data are often not complete to handle each type of problem or they are not able to totally remove their impact; the efficiency is also a function of the type of event.

In convective cases, attenuation, ground clutter, hail echo, melting zone, high dis-homogeneity in the DSD should be correctly considered to extract a valuable information from radar data and to avoid mistakes in radar images interpretation. In order to reduce such problems quality flags have been used in reconstruct radar fields (Fornasiero, 2006, Fornasiero et al. 2005).

Further, polarimetric Doppler C-Band radars are strategic instruments for the 3-D reconstruction of thunderstorms, allows to identify the prevailing hydrometeor type and their spatial distribution within the meteorological event and the dynamic evolution of the cloud system. A fuzzy logic hydrometeor classification scheme, developed at the National Severe Storms Laboratory (NSSL, Zrnic et al., 2001), and recently extended from S-band to C-band radar data (Marzano et al., 2006), is used to detect the microphysical structure the event.

To better localize the storm position and the locations damaged during its evolution the high-resolution Google-Earth visualization platform have been used (Smith and Lakshmanan 2006).

II. CASE STUDY ANALYSIS

On 3rd August 2006 a Supercell storm sweep over the Po Valley. Fig. 1 shows a time frame of such event and the associated quality index pattern. The occurrence of severe attenuation is highlighted in a cone-shape feature behind the storm core.

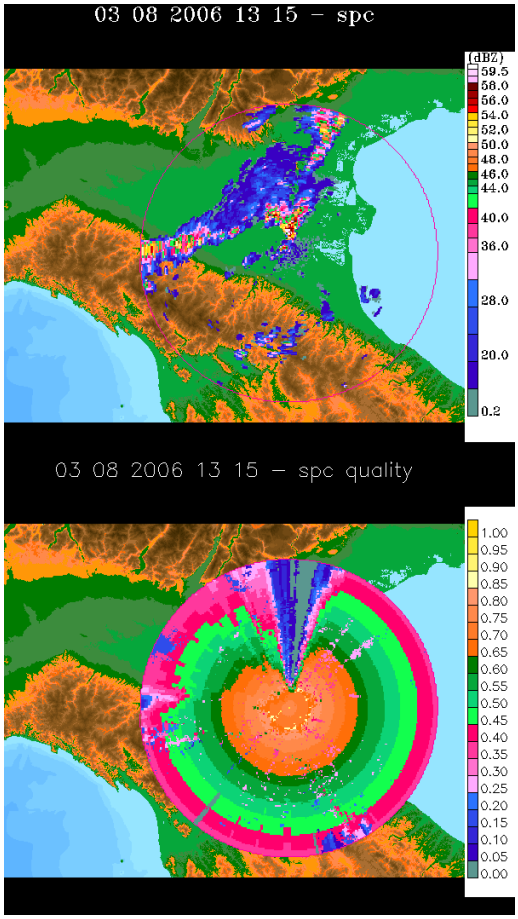

FIG. 1: 03-08-2006 13:15 UTC San Pietro Capofiume radar; (above) radar reflectivity map; (below) quality index map.

A first immediate advantage offered by the quality descriptor is that it 'warns' the data user about possible bad quality of data in some areas of radar fields and 'invites' him to critically consider the information in such areas; the second considerable advantage is that it permits to merge multiple radar data in a selective way, offering a method to

generate the 'best data' composed field.

The occurence of such a system, the strong winds associated and the hailfall are at the bottom of the heavy damge observed.

The Doppler analysis detected the presence of the typical Supercell vortex, while unfortunately the hydrometeor classification was limited by the strong attenuation phenomenon.

Radar products have been geo-located and visualized using the Google Earth platform, allowing a detailed analysis of the storm path and a comparison with damages report.

III. RESULTS AND CONCLUSIONS

The quality concept is applied to this Supercell case. An extended analysis, based on the informations extracted from the reflectivity radar data, has been carried out. The capability of the quality descriptor to improve the information extracted from radar data is hence discussed.

A meteorological description has been carried out and linked with the Doppler-polarimetric analysis of severe events, to complete event reconstructions.

Further Google-Earth as been applyed to provides an easy-to-use GIS platform that allows a easy real-time integration of different data, that can be very helpful in the operational application and monitoring.

IV. AKNOWLEDGMENTS

This activity is carried on in the framework of PROSCENIO and “Mosaicatura radar”.

V. REFERENCES

Fornasiero, A., 2006: On the uncertainty and quality of radar data. Ph.D. Thesis. Università degli studi della Basilicata.

Fornasiero A., Alberoni P. P., Amorati R., Ferraris L., Taramasso A. C., 2005: Effects of propagation conditions on radar beam-ground interaction: impact on data quality. ADGEO, 2, 201-208.

Marzano, F. S., D. Scaranari, M. Celano, P.P. Alberoni, G. Vulpiani and M. Montopoli, 2006: Hydrometeor Classification from dual-polarized weather radar: extending fuzzy logic from S-band to C-band data. *Adv. Geosci.*, **7**, 109-114.

Smith, T. M. and V. Lakshmanan, 2006: Utilizing Google Earth as a GIS platform for weather applications. 22th Int'l Conf. on Inter. Inf. Proc. Sys. (IIPS) for Meteor., Ocean., and Hydr., Atlanta, GA, Amer. Meteo. Soc., CD-ROM.

Zrnić, D. S., A. V. Ryzhkov, J. M. Straka, Y. Liu, and J. Vivekanandan, 2001: Testing a procedure for automatic classification of hydrometeor types. *J. Atmos. Oceanic Technol.*, **18**, 892-913.

UHF RADAR STUDIES OF VERTICAL MOTION AND TURBULENCE CHARACTERISTICS IN PRE-MONSOON THUNDERSTORM OVER AN INDIAN TROPICAL STATION

Sachin Deshpande[1] P. Ernest Raj[1]
[1]*Indian Institute of Tropical Meteorology, Pashan, Pune-411008, India, sachinmd@tropmet.res.in*

I. INTRODUCTION

One of the most elusive of the parameters required in diagnostic and prognostic studies of the atmosphere is the vertical motion. Vertical motions exert a profound influence on the distribution of clouds and on the occurrence of precipitation. They provide the mechanism for vertical transport of any atmospheric property and thus influence the distribution of mass momentum and energy. Wind profilers are the only instruments that can provide virtually continuous observations of vertical motion through a column within convection at scales that can accurately sample the convection itself. This together with information on horizontal winds hydrometeor fall velocities with high time and space resolution has been used to explore the relationship between air motions within the convective storm and the microphysics (May and Rajopadhyaya 1996).

II. PRESENTATION OF RESEARCH

The aim here is to present a case study observed with 404 MHz UHF radar/wind profiler data from a tropical land station Pune (18.31^0 N 73.58^0 E) during a pre-monsoon season severe convection event. The ability of wind profiler to directly measure vertical air motions and hydrometeor fall velocities through precipitating and non-precipitating systems has been explored through an analysis of the pre-monsoon thunderstorm which occurred in the evening hours on May 16 2004. Using the observed UHF radar data the extent of the enhancement in the vertical velocity horizontal wind shear and the turbulence distribution during the thunderstorm activity is discussed in this paper. Temporal variation of surface meteorological parameters before and during the thunderstorm event is also presented as supporting information.

III. RESULTS AND CONCLUSIONS

Time-height variation of vertical velocities (top panel) reflectivities calculated from the observed spectral signal to noise (SN) ratio (second panel) turbulence parameter (third panel) and horizontal wind shear (bottom panel) observed in the height range 1.05 km to 8 km for May 16 during 0800 to 2100 hrs local time obtained from Pune wind profiler are presented in Figure 1. The measured vertical velocity profiles show upward motions in the morning hours up to an altitude of 3 km. When the thunderstorm starts developing or gets initiated a strong downdraft with velocities between -1 m/sec to even -4 m/sec are seen in the height region of 3 to 10 km. In the growing stage the downdraft can be seen to be prevalent right from lowest observable heights of 1.05 km. It is observed that the precipitation signals (Rayleigh scattering) dominate the UHF signal during thunderstorm period. The reflectivity profiles during clear air conditions before thunderstorm activity were predominantly negative. The reflectivity increases by more than 0 dB as convective cloud starts developing after 1400 hrs. Reflectivities are as high as 20 dB once the heavy precipitation starts falling during the period 1800-2000 hrs. One can see the initiation of thunderstorm (around 1400 hrs) it vertical growth from 1400 to 1800 hrs from the upward sloping reflectivity contours. The vertical velocity fluctuations (given by S_w spectral width) show a region of strong turbulence (right from 1.05 km to 8 km in the vertical) with high S_w values during the growing and mature stage of the thunderstorm. Vertical shear of horizontal wind showed increased shear in the entire height region from 1.35 to 5 km during the peak activity of thunderstorm. Wind shears ranged between 0.01 and 0.03 m^2/sec^2 at the time of intense convection. Thunderstorm produces convective wind shear for a short period of time which is seen in this case study.

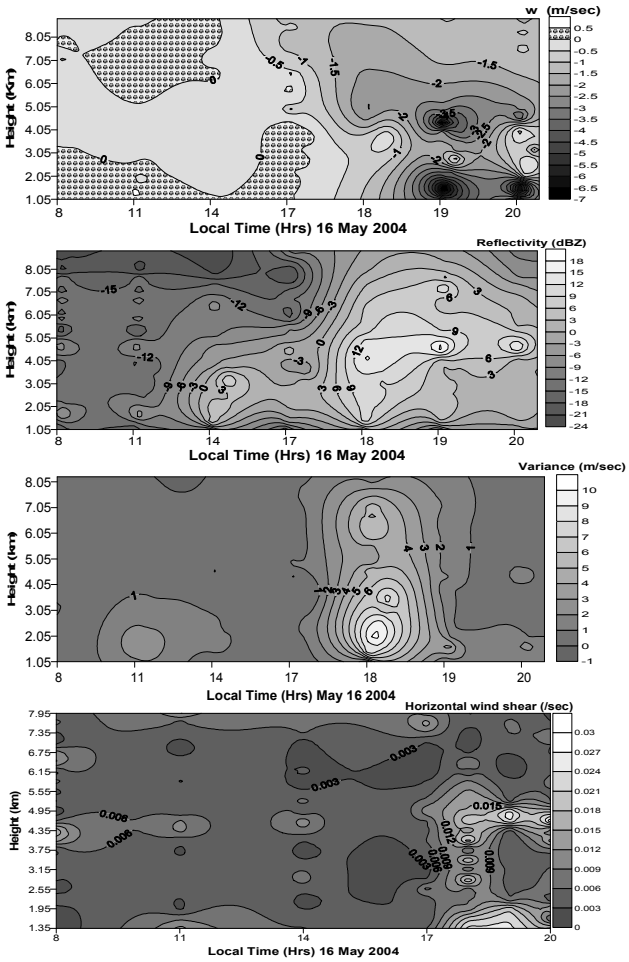

FIG 1: Time-height cross sections of vertical velocity (top panel) reflectivity (second panel) variance (third panel) and horizontal wind shear (bottom panel).

Surface meteorological parameters recorded at the wind profiler site namely Wind speed (hourly average and maximum during that one hour) hourly average Temperature Relative Humidity Pressure and total Rainfall during the hour are plotted and shown in Figure 2 for 16 May 2004 between 0800 and 2100 hrs LT.

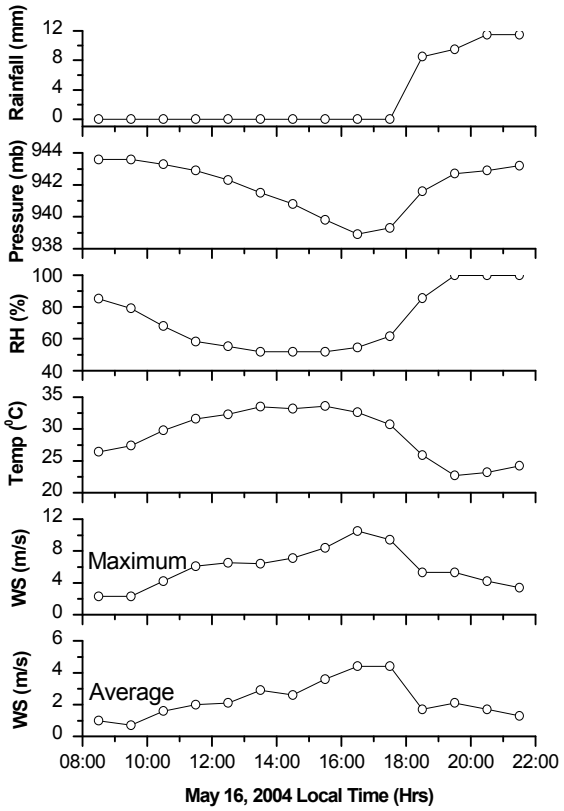

FIG 2: Surface meteorological parameters recorded at UHF radar site on May 16 2004.

Wind speeds were maximum in magnitude at the mature stage of the thunderstorm and the instantaneous values reached as high as 10-12 m/sec when thunderstorm was overhead and fully developed. Maximum surface temperature at this tropical station usually occurs around 1400 hrs LT but on this particular day the condition of maximum surface temperature extended by nearly two hours. Relative humidity started increasing just before precipitation occurred. Surface level pressure fell by about 7 mb and showed minimum at the mature stage of the thunderstorm. Thus all the surface meteorological parameters showed changes typical of the various stages of a tropical pre-monsoon thunderstorm. Data at shorter interval will be further analyzed to delineate the various stages in more detail.

The above case study during a pre-monsoon thunderstorm event over a tropical station shows number of different interesting features during period of atmospheric strong convection. These include large rapidly varying vertical velocities (updrafts and downdrafts) large values of vertical spectral width enhanced signal powers in the troposphere and associated low level wind shears changes in momentum fluxes during the life cycle of thunderstorm activity. As the radar echoes from UHF radars clearly distinguish those from hydrometeors and from clear air it is possible to ascertain the time when actual precipitation occurs. The UHF radars/wind profilers provide wind and turbulence information at high temporal and spatial resolution which enables one to study such events of intense convection in detail.

IV. AKNOWLEDGMENTS

The authors wish to thank the Director Indian Institute of Tropical Meteorology for his encouragement and support. Data of surface meteorological parameters has been obtained from India Meteorological Department Pune and the same is gratefully acknowledged.

V. REFERENCES

May P. T. Rajopadhyaya D.K. 1999: Vertical velocity characteristics of deep convection over Darwin Australia. *Mon. Wea. Rev.* 127 1056-1071.

WINDFIELD RECONSTRUCTION OVER CONVECTIVE STORMS BY USING ALONG-TRACK TECHNIQUE

Y. K. Goh[1], A. R. Holt[2], P. P. Alberoni[3] , G. Cenzon[4]

[1]*Department of Mathematical and Actuarial Sciences, Universiti Tunku Abdul Rahman,13 Jalan 13/6, 46200 Petaling Jaya, Selangor, Malaysia, gohyk@mail.utar.edu.my*

[2]*Department of Mathematical Sciences, University of Essex, Wivenhoe Park, Colchester CO4 3SQ, United Kingdom, anthony@essex.ac.uk*

[3]*A.R.P.A. - Servizio IdroMeteorologico, Viale Silvani 6, 40122 Bologna, Italy, palberoni@arpa.emr.it*

[4]*A.R.P.A.V. Centro Meteorologico di Teolo, Via Marconi 55, 35037 Teolo, Italy, gcenzon@arpa.veneto.it*

(Dated: September 12, 2007)

I. INTRODUCTION

Accurate windfield information is important for computational study on weather models. However, most windfield data from direct measurements have their own problems. For example, measurements from weather balloons are supposed to be the most accurate, but point measurements cannot give a good representation of overall windfield over a large area. In this case, radar Doppler wind measurements provide a good description of the windfield over a large area, and at the same time provide fine spatial resolution that cannot be achieved by satellite data. The main drawback of radar measurements is that they only give the radial component.

To overcome this problem, many have proposed techniques to construct the three dimensional windfield by either making ad hoc assumption, such as VAD (Lhermitte and Atlas 1961), or by requiring additional input, such as dual Doppler wind retrieval (Lhermitte 1970; Dowell and Shapiro 2003). In this paper, we will present a simple technique to allow fast construction of windfield from a region covered by three overlapping Doppler radars.

II. ALONG TRACK CALCULATION OF WINDFIELD

Here, we present a simple calculation to extract windfield information from three Italian Doppler radars. The three radars are located at Gattatico, GAT (44°47'30" N, 11°30'30" E), San Pietro Capofiume, SPC (44°39'17" N, 11°37'25" E), and Teolo, TEO (45°21'46" N, 11°40'25" E). The first two radars are belong to ARPA-EMR, the Civil Defend Agency of Emilia-Romagna region, and the last radar is belongs to ARPA-Veneto, the Civil Defend Agency of Veneto region.

Our strategy to construct the windfield is first we calculate the two horizontal along-track components of the windfield by considering two radars at a time. By *along-track*, we mean the component that parallels to the line joining the radars. Then the two along-track components will be transformed into a orthogonal coordinate system. Finally, the vertical component will be constructed by integrating the equation of continuity. A similar technique has been used by the authors to verify windfield retrieved by using dual-Doppler method (Goh 2006).

One of the advantages of this techniques is the algorithm is relatively simple to implement. It does not need to invoke any theory in order to obtain the horizontal windfield, and it does not have the problem that dual-Doppler wind retrieval has, where the regions around the straight lines connecting the radars are 'blind spots' of the retrieval. By using the along-track technique, it is possible to extract the wind components around this region.

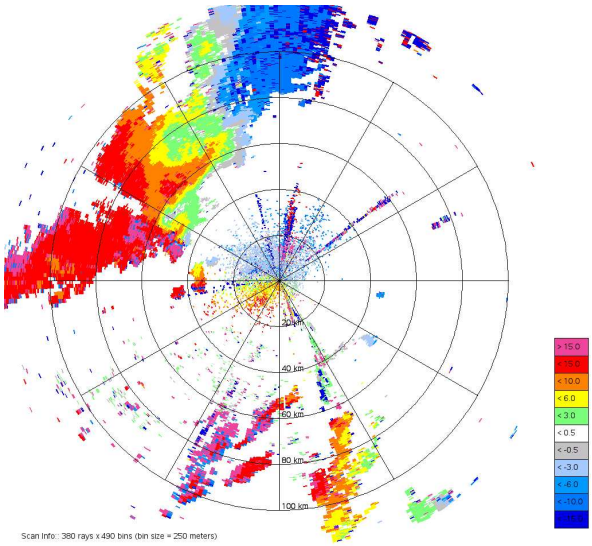

FIG. 1: Doppler velocity PPI picture from SPC radar on 3 August 2006, 1230UTC. Strong Doppler wind on the 40 km to 80km North-west region from the radar.

III. RESULTS AND CONCLUSIONS

We have identified an interesting convective storm event on 3 August 2006 (1100 UTC – 1400 UTC, Figure 1). We will present the windfields retrieve on these hours and compare with the windfields retrieved from dual-Doppler technique.

V. REFERENCES

Dowell, D. C., Shapiro, A., 2003: Stability of an iterative dual-Doppler wind synthesis in Cartesian coordinates, *J.*

Atmos. Oceanic Technol., **20**, 1552 – 1559.

Goh, Y. K., Holt, A. R., Alberoni, P. P., 2006: Radar windfield retrieval over the Po Valley, Nat. Hazards Earth Syst. Sci., 6 285 – 291.

Lhermitte, R. M., Atlas, D., 1961: Precipitation motion by pulse Doppler radar. *Proc. 9th Weather Radar Conf*., Amer. Meteor. Soc., 218 – 223.

Lhermitte, R. M., 1970: Dual-Doppler radar observations of convective storm circulation, in Preprint, *14th Conf. on Radar Meteorology*, Amer. Meteor. Soc., 153 – 156.

Detection of turbulence generated by convective motions by an X-Band Doppler Radar: The DTCOR Method

Fadela Kabeche (1,2), Alain Protat[1], Yvon Lemaître[1], Stéphane Kemkemian[2], Jean-Paul Artis[2]

1 *Centre d'Etude des Environnements terrestre et planétaires , 10-12, Avenue de l'Europe 78140 Vélizy-Villacoublay,France,Fadela.kabeche,Alain.protat,Yvon.lemaitre@cetp.ipsl.fr*

2 *Thalès systèmes Aéroportés, 1,bd Jean Moulin 78852 Elancourt Cedex,France,stephane.kemkemian,jean-paul.artis@fr.thalesgroup.com*

(Dated: September 12, 2007)

I. INTRODUCTION

Atmospheric turbulence, a scientific subject that challenges many research fields, has a direct impact on aviation safety and thus deserves a close investigation.[Proctor 2002]

Indeed, one of the most leading causes of in-flight injuries is atmospheric turbulence. The current state of the art of turbulence detection with radar doesn't efficiently detect and quantify aircraft turbulence hazards in areas characterized by small radar reflectivities[Hamilton 2002].

The present work is devoted to the development and evaluation of a new real-time detection method of turbulent structures generated by convection using Doppler information from an X-band radar. The typical size of these turbulent structures, whose impacts on aircrafts are meaningful, ranges between 100m and 3000m. These turbulent structures result from gravity waves triggered by convective activity and propagating horizontally outside this area far away (till several tens of kilometers).

This method is referred to hereafter as DTCOR (Detection of COnvective Turbulence by Radar) and described in Section II. Preliminary evaluation of the method is presented in Section III.

II. PRINCIPLE OF DTCOR:

The present version of the method considers that radar signals are available in the zone of turbulence. This version 1 of DTCOR can be described in three steps which in fact are performed simultaneously by using a variational mathematical formalism.

The first step retrieves the horizontal components of the wind (U,V) and the divergence term DIV= dU/dx + dV/dy from radial velocity measurements in a retrieval domain D located in front of the aircraft and in an horizontal sectorial scan (with null fixed elevation) performed by the radar. The distance of this zone D from the aircraft is chosen to allow a sufficient detection time of the turbulence prior to its penetration. The method also estimates the stretching deformation (DET= dU/dx - dV/dy) and the shearing deformation (DES= dU/dy + dV/dx) which can be also used to detect shearing zones produced by density currents or downbursts produced by storms (these zones can suddenly change the lift force during a landing). In the following, we will only consider the wind and the divergence components which can be used as a first alarm of strong turbulence (by a strong variability).

The horizontal components of the wind (U, V), the divergence (DIV), and the shearing deformation (DES) are retrieved by least square minimization between the radial velocities in the domain D and the analytical form of these radial velocities using a linearity assumption for the horizontal wind in the domain D (other assumptions such as quadratic or sinusoidal winds will be considered in the future). The interest of this assumption is that it requires a very low computational cost in agreement with the required real-time constraint.

Under this assumption, we can write the analytical form of the radial velocity:

$$Vr_i = \left(U_0 + U'_x(x_i - x_0) + U'_y(y_i - y_0)\right)\cos(az_i) + \left(V_0 + V'_x(x_i - x_0) + V'_y(y_i - y_0)\right)\sin(az_i) \quad (2.1)$$

with (x_0, y_0) the coordinates of the centre of the domain D, (U_0, V_0) the horizontal wind at the point (x_0, y_0), U'_x, V'_x, U'_y and V'_y are first derivatives of U and V with respect to x and y respectively.

This Equation (2.1) can be rewritten:

$$Vr_i = b_1\cos(az_i) + b_2\sin(az_i) + b_3(x_i - x_0)\cos(az_i) + b_4(y_i - y_0)\cos(az_i) + b_5(x_i - x_0)\sin(az_i) + b_6(y_i - y_0)\sin(az_i) \quad (2.2)$$

where $b_1 = U_0$, $b_2 = V_0$, $b_3 = U'_x$, $b_4 = U'_y$, $b_5 = V'_x$, $b_6 = V'_y$

We can show that the only attainable terms are b1, b2, b3, b6 and (b4+b5).

To obtain these b_k and thus the two components of the wind U,V, DIV, DES and DET a least square minimization is done between the measured radial velocities Vr_i in the domain D and the analytical form of these radial velocities expressed by eq (2.2):

$$S = \sum_i \left(\hat{Vr}_i - Vr_i\right)^2 \quad (2.3)$$

This minimisation of S with respect to the unknown bk ($\frac{\partial S}{\partial b_1} = 0$, $\frac{\partial S}{\partial b_2} = 0$, …and $\frac{\partial S}{\partial b_6} = 0$) leads to a linear system of M equations writing as: A.B= C

Where:

A is a matrix containing analytical information (MxM)

B is a vector of the unknown parameters (1xM)

C is a vector containing measured radial velocities (1xM).

The second step used the mass continuity equation for ice (or water) content Q derived from the measured radar reflectivity Z using an empirical relation (Q(Z)). This equation can be written:

$$\frac{DQ}{DT} = \frac{dQ}{dt} + U\frac{dQ}{dx} + V\frac{dQ}{dy} + (W - V_T)\frac{dQ}{dZ} = 0 \quad (2.4)$$

Where V_T is the terminal velocity of fall also derived from Z.

The simplified assumption used to establish this equation is that the process of condensation or evaporation is slow compared to the radar sampling time scale. Other

simplifications of this equation can be also considered according to the magnitude of horizontal variations of Q compared to vertical ones.
Thus this equation allows us to estimate W from the two wind components, U and V, and from two measurements of Z in time and according to the vertical.
In this case, two sectorial scans with two distinct elevations or several successive scannings during the aircraft flight are needed.
The last and third step consists in using the continuity equation of air mass linking the vertical wind W to horizontal divergence DIV:

$$\frac{dW}{dz} - \frac{W}{H} = DIV$$ where H is a height scale.

These three steps are performed simultaneously using a variational formalism with constraints (least square minimization of radial velocity, mass continuity equation Q and continuity equation).

III. RESULTS AND CONCLUSIONS

To evaluate DTCOR, a software simulating the aircraft flight pattern and the radar sampling has been developed. This software generates radial velocities from given wind and reflectivity fields verifying the previous physical constraints. An example of evaluation is given in the following. Others examples using more complicated fields deduced from numerical simulations performed using a cloud-system-resolving model will be discuss during the conference.
The total considered domain is

$$x \in [x_{\min}, x_{\max}] = [0, 75] \quad (km)$$
$$y \in [y_{\min}, y_{\max}] = [-40, 40] \quad (km)$$
$$z \in [z_{\min}, z_{\max}] = [0.19, 7.89] \quad (km)$$

The resolutions of the grid following x, y and z are respectively, $\Delta x = 0.5km$, $\Delta y = 0.5km$ and $\Delta z = 0.35km$.
The used three-dimensional wind field is [Protat 1998]:

$$U = A_1(1 - \frac{z}{H})\sin(\frac{2\pi}{\lambda}x)$$

$$V = A_2(1 - \frac{z}{H})\sin(\frac{2\pi}{\lambda}y)$$

$$W = z\left[\left(\frac{2\pi A_2}{\lambda}\sin(\frac{2\pi}{\lambda}y)\right) - \left(\frac{2\pi A_1}{\lambda}\sin(\frac{2\pi}{\lambda}x)\right)\right]$$

Where: H is scale height; A1 and A2 are constants to be defined; λ is a wavelength taken in the interval of turbulence between 50m and 3000m (the wavelength where a plane is most sensitive is around 400m).
This illustration will be given using the following parameters: A1 = A2=5m/s H = 8km and $\lambda = 40$km.
-The radar is in front of the aircraft
-The characteristics of the scanning are:
- Horizontal sectorial scanning
-Sampling in azimuth: -30° to 30° by step of 3°
-Elevation fixed to 0°.
The figure1 gives on a horizontal cross section the corresponding three-dimensional field on the total sampled domain.
Figure 2 give the retrieved wind field (in blue) superimposed on the initial one in the domain D of 8km x 8km centred at (x_0, y_0) = (40, 0) (i.e. 40km ahead of the aircraft).
As explained previously, the assumption used in the present retrieval is the linearity of the wind field in D. The validity of this assumption is of course mainly dependent on the size of D compared to the considered wavelengths and sensitivity of the retrieval accuracy to this size is presently being evaluated and will be discussed at the conference. The quality of this retrieval depends also on the co-linearity of the radial velocities in this domain D and thus depends on the size of D and its distance to the radar.
Figure 2 shows a good agreement between the simulated and retrieved wind field even if some significant differences are observed in some places, owing to departures from the linear assumption (because the first derivatives of the initial wind are not constant but are sinusoidal).
The quality of the retrieval can be improved using several scans carried out by the radar during the aircraft flight.

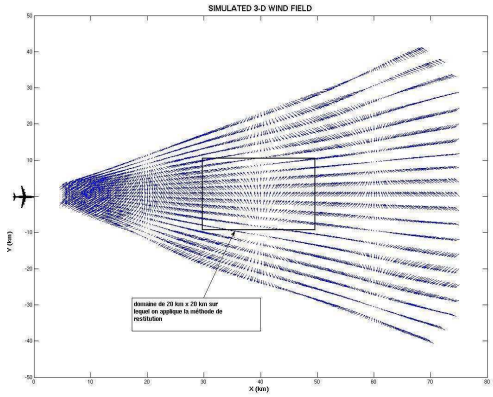

FIG. 1: Horizontal cross section of three dimensional fields

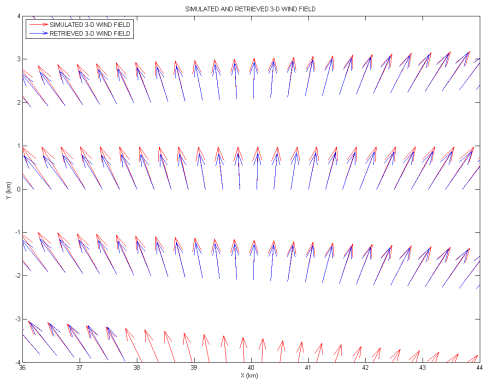

FIG. 2: Horizontal cross section of retrieved and simulated field

V. REFERENCES

Proctor, F.H., Hamilton D.W., and R.L. Bowles, 2002: Numerical Study of a Convective Turbulence Encounter. *40th Aerospace Sciences Meeting & Exhibit,* 14-17 January, Reno, NV, AIAA Paper No. 2002-0944, 12pp.

Protat A., Lemaître Y., Scialom G., 1998 :thermodynamical analytical field from doppler radar data by means of the MANDOP. analysis.Quart. *J. Roy. Meteor.Soc*., 124, 1663-1668.

Hamilton, D.W. and Proctor F.H., 2002: Meteorology Associated with Turbulence Encounters during NASA's Fall-2000 *Flight Experiments. 40th Aerospace Sciences Meeting & Exhibit,* 14-17 January, Reno, NV, AIAA Paper No. 2002-0943, 11pp.

SIGNATURES OF SEVERE THUNDERSTORMS FOR NOWCASTING IN THE STATE OF SÃO PAULO, BRAZIL

Gerhard Held[1], Ana Maria Gomes[1], Kleber P Naccarato[2] and Osmar Pinto Jr[2]

[1] Instituto de Pesquisas Meteorológicas, Universidade Estadual Paulista, Bauru, S.P., Brazil
gerhard@ipmet.unesp.br; ana@ipmet.unesp.br
[2] Grupo de Eletricidade Atmosférica, Instituto de Pesquisas Espaciais, São José dos Campos, S.P, Brazil
kleberp@dge.inpe.br; osmar@dge.inpe.br
(Dated: September 12, 2007)

I. INTRODUCTION

The Instituto de Pesquisas Meteorológicas (IPMet) of the Universidade Estadual Paulista has observed the three-dimensional structure of severe thunderstorms, including the radial velocities inside and near these storms, since 1992 and 1994, respectively, using two S-band Doppler radars in Bauru and Presidente Prudente, in the central and western part of the State of São Paulo (Figure 1). Criteria for the early detection of severe wind and hailstorms have been sought and are already, at least in part, incorporated in the real-time monitoring and alert system. However, research into the relationship between radar echoes and lightning discharges only commenced in 2004. Findings from two storm days with three confirmed tornadoes and two supercell storms within radar range are presented, using NCAR's (National Center for Atmospheric Research) TITAN (Thunderstorm Identification Tracking Analysis and Nowcasting; Dixon and Wiener, 1993) Software, which had been implemented at IPMet and adapted for local requirements in 2005/2006.

The ultimate goal of this study is to derive characteristic signatures, which could aid the nowcaster to identify severe weather and disseminate early warnings to Civil Defense Organizations, the electricity sector and the public.

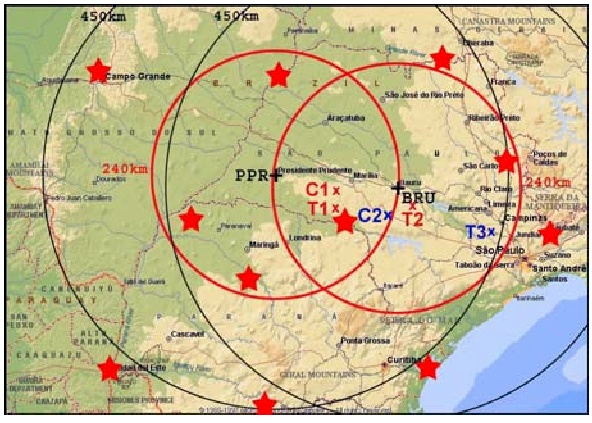

FIG. 1: IPMet's Radar Network (BRU = Bauru; PPR = Presidente Prudente), showing 240 and 450 km range rings. The areas where the tornadoes occurred are marked T1 (Palmital), T2 (Lençois) and T3 (Indaiatuba). C1 and C2 are severe storm cells moving on parallel tracks of T1 and T3, respectively. Lightning sensors are marked in red.

II. METHOD

IPMet's radars have a range of 450km for surveillance, but when operated in volume-scan mode every 7.5 minutes it is limited to 240km, with a resolution of 1km radially and 1° in azimuth, recording reflectivities and radial velocities. In this study, the reflectivity threshold was set at 10 dBZ. The Brazilian Lightning Detection Network currently comprises 24 sensors in total (some are outside the area shown in Figure 1), with a detection efficiency of 80-90 % (CG = Cloud-Ground strokes only) and a location accuracy of 0.5-2.0 km (Pinto Jr., 2003).

TITAN produces a variety of important parameters for a chosen reflectivity and volume threshold throughout the lifetime of storms, such as Area, Volume, Precipitation Flux, VIL (Vertically Integrated Liquid water content), Maximum Reflectivity, Hail Metrics, speeds and direction of propagation, etc, per volume scan. It also has the facility to collocate flashes with the radar echoes, including a separation into positive and negative strokes.

III. OBSERVATIONS AND RESULTS

Until recently, tornadoes were believed to be rather rare and exceptional events in Brazil, and very few radar observations had been available. The only Doppler radar observations of a tornado occurring in the State of São Paulo before 2004 were reported in Gomes *et al.* (2000). However, during May 2004 and 2005, three confirmed tornado-spawning storms and a supercell storm were observed in the State of São Paulo by IPMet's S-band Doppler radars. Since they occurred during the southern hemisphere autumn, the cells were not amongst the most intense in terms of radar reflectivity (50-60 dBZ) and their echo tops rarely exceeded 12 km, but they exhibited extremely strong radial velocities and rotational shear (up to $-5.0 \times 10^{-2} s^{-1}$), which initiated a cyclonic vortex in the center of the cells, spawning the tornadoes. One of the severe cells (C1) was classified as a supercell storm, based on its long life cycle of more than 8.5 hours (Figure 2). It had almost identical characteristics as its tornadic partner cell (T1), except for a Weak-Echo-Region.

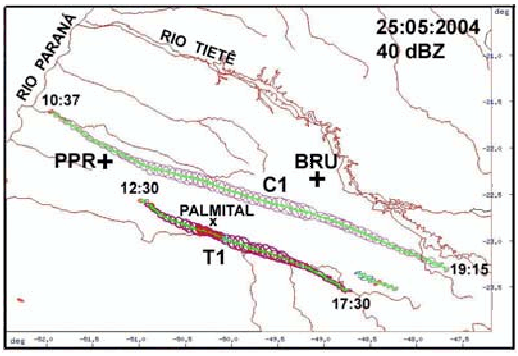

FIG. 2: Composite radar image, showing the tracks of 40 dBZ centroids of supercell C1 and tornadic cell T1 (Palmital) on 25 May 2004. Times of first and last detection in local time (LT). Not all simultaneous tracks are shown. Red centroids indicate the confirmed tornado touch-down.

Conventional Doppler radar observations had already identified cell motion of >50 km.h^{-1}, VIL (Vertical Integrated Liquid water), Weak Echo Regions, hook echoes (Markowski, 2002) and strong rotational shear as good indicators of possible severe storms in Southeast Brazil, including tornadoes (Held *et al.,* 2005). However, TITAN yields the temporal history of many severe storm indicators along all cell tracks, providing valuable signatures for Nowcasting. When subjected to TITAN analysis, the supercell revealed much greater severity parameters (VIL=70.6 kg.m^{-2}, MAX-Z=≥60 dBZ, VOL = 500 to >1000km^3 sustained for four hours; Figure 3), than the tornadic cells, but no reports of damage or the formation of another tornado were received. The temporal evolution of VIL values shows a rapid decrease close to the time of the observed destructive winds at ground level (e.g., tornado touch-down; T3, Figure 4), but the highest values of VIL were not necessarily observed close to the time of the tornado touch-down.

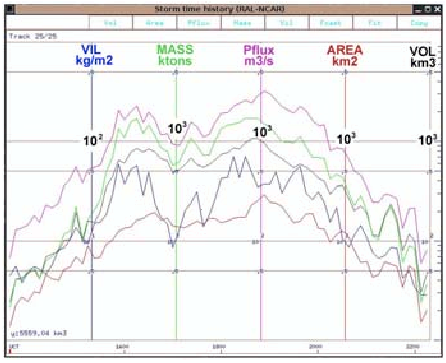

FIG. 3: 25 May 2004: Storm Time History of supercell C1 from 10:45 – 19:15 LT.

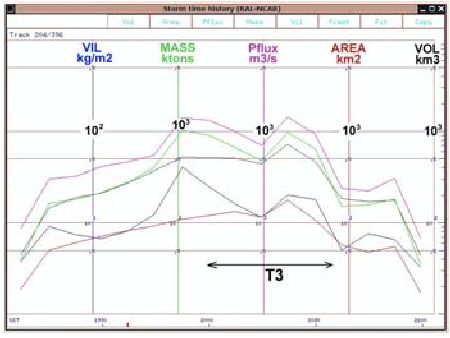

FIG. 4: 24 May 2005: Storm Time History of tornadic cell T3 during the second half of its life time (16:08 - 18:00 LT).

Analysis of lightning records, superimposed on radar images indicated a preferential location of CGs around or ahead of the core of tornadic cells, while in the supercells the CGs were observed within and around the core and with greater frequency. Lightning activity almost ceased shortly before the touch-down of the tornadoes (Figure 5), which is in agreement with observations of tornadoes and supercell storms in Oklahoma (Rison *et al*., 2005). No significant differences of lightning parameters (peak current, multiplicity, polarity) were found for the tornadic and non-tornadic cells. However, flash polarity seems to be a good discriminator between mature convective cells and stratiform rain regions, with the latter producing only few and mostly positive flashes, while even slowly decaying convective cells may still generate large numbers of flashes, but an increasing portion is positive.

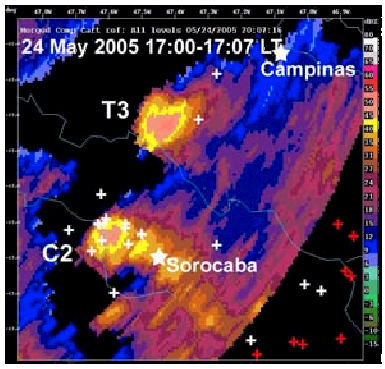

FIG. 5: 24 May 2005: Position of CG strokes (+ negative; + positive) relative to the echo core of storm T3 during the tornado activity, as well as for supercell C2, during a 7.5 min interval.

IV. CONCLUSION

TITAN radar products are already operationally available to IPMet's meteorologists in real time, but mechanisms and algorithms still need to be developed for an automatic alert system. If high-resolution lightning data were also available in real time, they could be integrated into the radar images, yielding a powerful Nowcasting system, with vast benefits, not only for Civil Defense Authorities and the public, but for the agricultural and electricity sectors.

V. ACKNOWLEDGMENTS

Hermes A.G. França is thanked for assisting with the retrieval and pre-processing of the raw radar data. Drs Jim Wilson and Mike Dixon, as well as Niles Oien of the National Center for Atmospheric Research are gratefully acknowledged for facilitating the implementation and application of the TITAN and CIDD software packages at IPMet, being maintained by Jaqueline M. Kokitsu.

VI. REFERENCES

Dixon M. and Wiener G., "TITAN: Thunderstorm Identification, Tracking, Analysis & Nowcasting - A radar-based methodology", *J. Atmos. Oceanic Technol*., **10**, 785-797, 1993.

Gomes, A. M., Held, G, Lima, M. A. and Calheiros R.V., 2000: Estudo da Evolução de Tempestades Severas na Área Central do Estado de São Paulo por Radar Doppler. *Proceedings, XI Congresso Bras. de Meteor.*, SBMET, Rio de Janeiro, Oct. 2000, Paper MR00006, 1921-1929.

Held G., Gomes A.M., Naccarato K.P., Pinto Jr. O, Nascimento E., Correia A.A. and Marcelino I.P.V.O., 2005: "Analysis of Tornado Characteristics in the State of São Paulo for the Improvement of an Automatic Alert System", *Preprints, 32nd Conference on Radar Meteorology,* Paper P3R.9*,* 10pp, AMS, Albuquerque, USA, October 2005.

Markowski, P. M., 2002: Hook echoes and rear-flank downdrafts: a review. *Mon. Wea. Rev*., 130, 852-876.

Pinto Jr., O., 2003: The Brazilian lightning detection network: a historical background and future perspectives. *Proc., VII International Symposium on Lightning Protection*, Curitiba, Brazil, Nov. 2003, 3-5.

Rison W., Krehbiel P., Thomas R.J. and Hamlin T., 2005: Three-dimensional lightning mapping observations as a compliment to radar observations of storms, *Preprints, 32nd Conference on Radar Meteorology,* Poster JP3J.23, AMS, Albuquerque, USA, Oct. 2005.

HAIL CELLS FEATURES AND PROBABILITY OF HAIL EQUATIONS IN THE REGION OF EBRO VALLEY

Manuel Ceperuelo[1], María del Carmen Llasat[1], Tomeu Rigo[2], José Luís Sánchez[3]

[1]*Department of Astronomy and Meteorology, University of Barcelona, Spain, ceperuel@am.ub.es*

[2]*Meteorological Service of Catalonia, Generalitat de Catalunya, Spain*

[3]*Laboratory for Atmospheric Physics, University of León, Spain*

(Dated: September 12, 2007)

I. INTRODUCTION

Hail events are typically related to crop losses, buildings and cars damages or casualties. Different kinds of techniques are used in order to identify hail and to help risk management. There exist methods that try to find different relationships between environmental conditions and radar observations (Stumpf et al, 2004) with the purpose to identify hail in surface, for example, the use of maximum reflectivity (Geotis, 1963), the persistence of maximum reflectivity values (Knight et al, 1982; Waldvogel et al, 1987), the use of radar data combined with radiosonde observations (Edwards and Thompson, 1998; Waldvogel et al, 1979), VIL technique (Greene and Clark, 1972) and VIL density method (Amburn and Wolf, 1997), the use of kinetic energy flux (Waldvogel et al, 1978; Schmid et al, 1992), the hail detection algorithm (Witt et al, 1998), the use of logistic functions that try to minimise the false alarm ratio (Billet et al, 1997) or by using the combination of different hail indicators (Kessinger and Brandes, 1995).

The objective of this contribution is to obtain the best relationship between hail observations and radar parameters in case of Ebro Valley region, NE of Spain (Fig. 1). This area is usually affected by spring and summer hail storms mainly in the south-western part with an average of 32 thunderstorm days per year over an area of 25000 km^2 and a medium size of hailstones less than 20 mm (Pascual, 2000; López, 2003), which are usually registered around 16:00 UTC. To achieve this end, 2004 and 2005 hail campaigns (from May to September) have been analysed. During these periods, a number of 814 ground hail observations corresponding to 70 hail events have been produced and the largest recorded hailstones have had a size of 43.9 mm (2004) and 39.4 mm (2005).

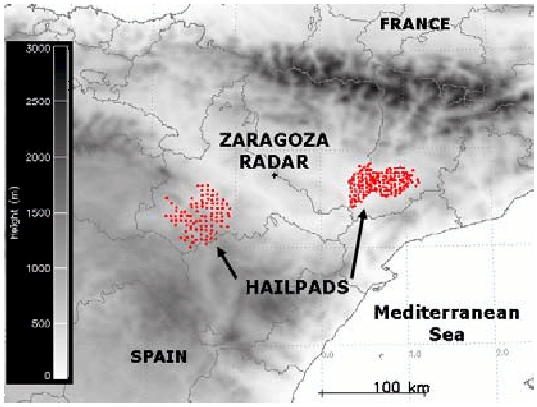

FIG. 1: Ebro valley region, radar location and hailpad networks.

This contribution shows the 3D cells analysis obtained by using RHAP, Rainfall events and Hailstorms Analysis Program (Ceperuelo et al, 2006), which has an adapted version of the SCIT algorithm (Johnson et al, 1998; Rigo and Llasat, 2005), and integrates meteorological radar data, meteorological model outputs, radiosonde observations and surface observations, like hailpads. Finally, conclusions are presented.

II. CONVECTIVE CELLS ANALYSIS

A total number of 9537 convective cells have been identified, and 4863 of them (51%) have been detected within the valid radar range: (20-150 km). Moreover, taking into account the hailpad areas and hail events, 706 convective cells affected these regions and 25% of them produced hail in surface. In hailpads areas, the maximum storm formation occurrence (MSO) has been obtained between 17 and 19 UTC, two hours before the MSO of the all Ebro Valley region (15 UTC - 16 UTC). In case of hailpad areas, the analysis shows: 1) no hail cells displacements have a Gamma distribution with medium value of 21.4 km and a pronounced maximum between 4 and 8 km; 2) hail cells have a medium displacement value of 46.8 km and two maxima between 15 and 20 km and between 30 and 35 km. This fact is due to a major organisation of the associated precipitation system in hail case. Considering 3D cells direction, the mean value is similar for both cases, nonetheless hail cells have more SW-NE component.

On the other hand, the evaluation of the radar parameters has been done in order to obtain the best parameter to identify hail or no-hail in surface. For this purpose, contingency tables and the score indexes have been built. Results can be summarised in table I, which shows that there are no significance differences between the most important radar parameters related with hail precipitation. Then, considering hail and no hail observations, probability of hail equations have been constructed (table II) and might be used taking into account the obtained score indexes.

This study gives the kinetic energy flux (KEF) as the best parameter to identify hail in surface with a linear function to model the hail probability. Moreover, if only hail larger than 10mm is considered, an adapted version of the probability of severe hail (POSH) has been shown as the best parameter to identify it (table II, figure 2). This adapted version has been obtained for the Ebro Valley region on the basis of 10 severe hail events and is based on the Hail Detection Algorithm (Witt et al, 1998).

Radar parameter	CSI	Value
Zmax	0.3776	52.0d BZ
WP	0.3633	3.5 km
VIL_{Zmax}	0.3795	16.0 kg/m^2
VIL_{grid}	0.3753	14.0 kg/m^2
VIL_{cell}	0.3473	12.0 kg/m^2
$VILD_{Zmax}$	0.3734	2.0 g/m^3
$VILD_{cell}$	0.3170	1.8 g/m^3
KEF	0.3929	0.5 J/m^2/s
SHP	0.3976	0.5

TABLE I: Highest critical success index (CSI), and corresponding value to identify hail and no hail cells.

Radar parameter	a	b	c
Zmax	0.0001	0.155	-0.062
WP	0.200	0.184	-0.111
VIL_{Zmax}	0.018	-0.009	non
VIL_{grid}	0.017	0.069	non
VIL_{cell}	0.023	0.044	non
$VILD_{Zmax}$	0.179	-0.106	non
$VILD_{cell}$	0.242	-0.079	non
KEF	0.333	0.135	non
POSH	0.0001	0.155	-0.062

TABLE II: Parameters for exponential ($POH = a \cdot e^{bx} + c$) and linear ($POH = a \cdot x + b$) distributions of hail probability (X is the radar parameter).

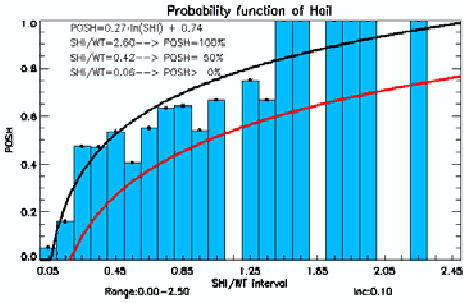

FIG. 2: POSH distribution for the region of Ebro Valley, black line, and POSH distribution obtained by Witt et al. (1998), red line.

III. RESULTS AND CONCLUSIONS

After analysing 46 hail events, a total number of 9537 hail and no hail cells have been detected. Mean directions of the cells movement have no significant differences, with WSW-ENE as the mean direction. Hail cells have displacements longer than no-hail cells, with mean values of 46.8km and 21.4km respectively. This fact agrees with the organisation degree of the precipitation systems with hail, which leads us to see the MUL system as those with the highest hail probability.

The KEF parameter with a linear distribution of hail probability is the best parameter to identify hail in surface, nonetheless there exist no significance differences with the other radar parameters. When hail size is larger than 10 mm the best parameter is the adapted version of POSH for the region of Ebro Valley. These results joined to the dependence found between some radar parameters lead us to apply a new methodology based on principal components analysis, in order to improve the distinction between hail and no-hail cells. Then, the methodology will be applied to realize a cluster analysis of all the 3D cells to model the life cycle of the radar parameters.

IV. AKNOWLEDGMENTS

The authors thank the MONEGRO (REN2003-09617-C02-02) Spanish project for enabling the drawing up and presentation of this contribution. Our thanks to the Associació de Defensa dels Vegetals, to the University of Leon and to the Instituto Nacional de Meteorología for the hailpad data and radar data.

V. REFERENCES

Amburn S., Wolf P., 1997: VIL Density as a Hail indicator. *Wea. Forecasting*, 12, 473-478.

Billet J. M., DeLisi, Smith B.G., 1997: Use of regression techniques to predict hail size and the probability of large hail. *Wea. Forecasting*, 12, 154-164.

Ceperuelo M., Llasat M.C., Rigo T., 2006: Rainfall events and Hailstorm Analysis Program, RHAP. *Ad. Geo.*, 7, 205–213.

Edwards R., Thompson R. L., 1998: Nationwide Comparisons of Hail Size with WSR-88D Vertically Integrated Liquid Water and Derived Thermodynamic Sounding Data. *Wea. Forecasting*, 13, 277-285.

Geotis S.G., 1963. Some radar measurements of hailstorms. *J. Appl. Meteorol.*, 2, 270–275.

Greene D. R., Clark R .A., 1972: Vertically Integrated Liquid: a new analysis tool. *Mon. Wea. Rev.*, 100, 548-552.

Johnson J. Y, MacKeen P. L., Witt A., Mitchell E. D., Stumpf G. J., Eilts M. D., Thomas K. W., 1998: The Storm Cell Identification and Tracking (SCIT) Algorithm: An Enhanced WSR-88D Algorithm. *Wea. Forecasting*, 13, 263-276.

Kessinger C. J., E. A. Brandes, 1995: A comparison of hail detection algorithms. Final report to the FAA, 52pp. 1995.

Knight C.A., Smith P., Wade C., 1982: Storm types and some radar reflectivity characteristics. The National Hail Research Experiment, P. Squires and C. A. Knight, Eds., Vol. 1, Hailstorms of the Central High Plains, Colorado Associated University Press, 81–93.

López L., 2003: Convección atmosférica severa: pronóstico e identificación de tormentas con granizo. Doctoral Thesis, University of León, 207pp.

Pascual R., 2000: Granizo en el llano de Lleida. INM. Tempoweb training module.

Rigo, T., Llasat, M. C., 2005: Radar analysis of the life cycle of Mesoscale Convective Systems during the 10 June 2000 event. *Nat. Hazards Earth Syst. Sci.*, 5, 959–970.

Schmid W., Schiesser H. H., Waldvogel A., 1992. The kinetic energy of hailfalls: Part IV. Patterns of hailpad and radar data. *J. Appl. Meteorol.*, 31, 1165–1178.

Stumpf G. J., Smith T. M., Hocker J., 2004: New Hail Diagnostic Parameters Dervied by Integrating Multiple Radars and Multiple Sensors. Preprints, 22nd Conf. on Severe Local Storms, Hyannis, MA, Amer. Meteor. Soc., P7.8 - CD preprints.

Waldvogel A., Federer B., Grimm P., 1979: Criteria for the detection of hail. *J. Appl. Meteor.*, 16, 1521-1525.

Waldvogel A., Federer B., Schmid W., Mezeix J. F., 1978: The kinetic energy of hailfalls. Part II. Radar and hailpads. *J. Appl. Meteor.*, 17, 1680–1693.

Waldvogel A., Klein L., Musil D. J., Smith P. L., 1987: Characteristics of radar-identified big drop zones in Swiss hailstorms. *J. Climate Appl. Meteor.*, 26, 861–877.

Witt A., Eilts M. D., Stumpf G. J., Johnson J. T., Mitchell E. D., Thomas K. W., 1998: An enhanced hail detection algorithm for the WSR-88D. *Wea. Forecasting*, 13, 286–303.

QUANTITATIVE PRECIPITATION FORECAST USING RADAR ECHO EXTRAPOLATION

Petr Novák[1], Lucie Březková[2], Petr Frolík[3], Milan Šálek[4]

[1] *Czech Hydrometeorological Institute, Radar Department, Na Šabatce 17, 143 06 Prague, Czech Republic, petr.novak@chmi.cz*

[2] *Czech Hydrometeorological Institute, Regional office Brno, Department of Hydrology, Kroftova 43, 616 67 Brno, Czech Republic, lucie.brezkova@chmi.cz*

[3] *Czech Hydrometeorological Institute, Radar Department, Na Šabatce 17, 143 06 Prague, Czech Republic, petr.frolik@chmi.cz*

[4] *Czech Hydrometeorological Institute, Regional office Brno, Department of Meteorology, Kroftova 43, 616 67 Brno, Czech Republic, salek@chmi.cz*

(Dated: April 30, 2007)

I. INTRODUCTION

Radar echo extrapolation technique COTREC (Novák, 2007) is calculated operationally in the Czech Hydrometeorological Institute (CHMI) since 2003. These extrapolations are routinely used qualitatively for precipitation and severe weather nowcasting.

Accurate quantitative precipitation forecast (QPF) is highly demanded by operational hydrologist. QPF calculated from extrapolated radar fields could give for several first hours better results than forecasts from NWP models whose results are widely used as a precipitation input into the hydrological models. This paper presents work that tries to verify this hypothesis for Czech Republic territory.

II. PRESENTATION OF RESEARCH

COTREC method calculates motion vector field by comparison two consecutive Czech radar composites of maximum reflectivity. Acquired motion field is applied to PseudoCAPPI 2km composite for QPF calculation unlike maximum reflectivity for qualitative use. Extrapolated radar fields are accumulated for 0-1h, 1-2h and 2-3h time intervals and adjusted by the coefficient taken from radar-raingauge merge algorithm (Šálek *et al.*, 2004). Subsequently, mean and maximum precipitations over predefined catchments are calculated from these QPFs.

ALADIN NWP model (ALADIN, 2004) is operationally run in the CHMI. At present forecasts are calculated at 00, 06, 12 and 18 UTC but for dates presented in this paper forecasts were calculated only at 00 and 12 UTC and were available in approx. the third hour after start time. Forecasts are calculated in 1h step up to 54h. ALADIN is the main numerical model for short range forecast in the CHMI and is also used as an input into hydrological models.

The possible QPF improvement based on inclusion of COTREC method was evaluated on the extreme flood that occurred 30.6.-1.7.2006 in Dyje catchment. This event represents large-scale flash flood. The maximum precipitation, which hit the catchment within ten hours, was measured in Slavonice raingauge station and reached 150 mm, while the peak discharge in Podhradí profile (catchment area 1765 km^2) exceeded 100 years return time period.

The operation discharge forecasts based only on ALADIN precipitation forecast was compared with the discharge forecasts using COTREC QPF for first 3 hours. Even if the hydrological simulation of this type of flood event is very difficult, with the help of COTREC QPF it would have been possible to estimate the steep raise of water level several hours in advance.

So far, COTREC QPF was tested in Czech Republic as an input of a hydrological model HYDROG only for small catchments (Šálek et al. 2006). This work shows its considerable benefit even for catchments with area about hundreds to thousands km^2.

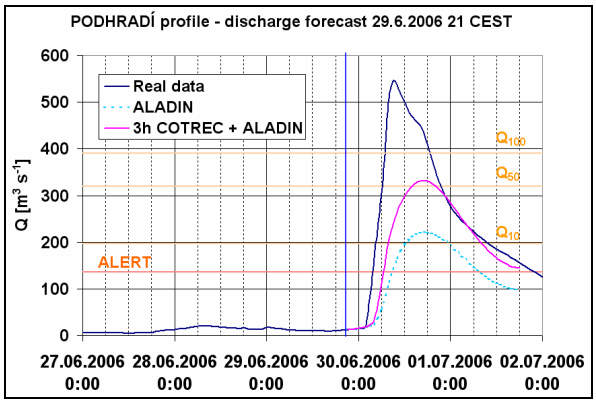

(a)

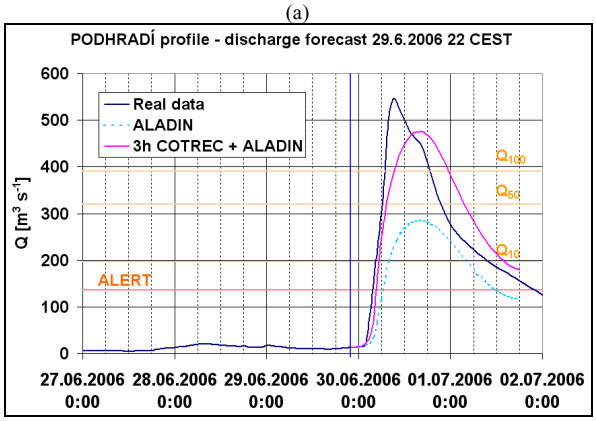

(b)

FIG. 1: Discharge forecasts at Podhradí profile, 29.6.2006 21:00 (a) and 22:00 (b) CEST. Figures show comparison of forecasts based on ALADIN data only and forecasts that use COTREC QPF for first 3 hours.

To make even deeper comparison of COTREC and ALADIN QPFs quality, data from 1.4.2006 to 30.9.2006 were investigated. RMSE, correlation coefficient and skill

scores (POD, FAR, CSI) were calculated for single catchments and also for whole area of Czech Republic. Quality of forecasts differs due to many factors including dependence on precipitation type, catchment area and location, but in most cases COTREC gives better results up to 2 hours. Fig. 2 shows example of this comparison where RMSE of forecasts were evaluated for each months from selected interval over the whole Czech Republic (calculated as an average of RMSE for all catchments on Czech territory).

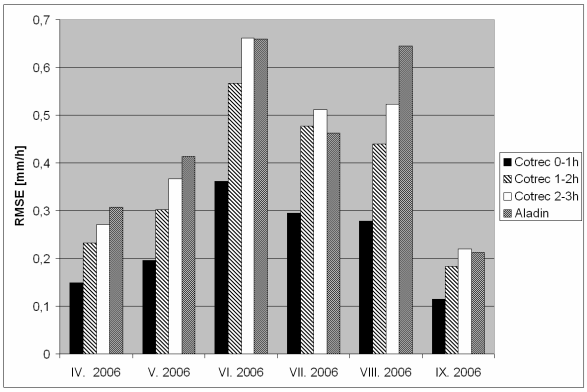

FIG. 2: RMSE comparison of 1h QPF by COTREC and QPF by ALADIN averaged over whole Czech Republic.

III. RESULTS AND CONCLUSIONS

Extreme flash flood case study and long-term statistical comparisons showed that COTREC QPF gives better results than NWP model QPF for 0-1h and 1-2h forecast and similar results for 2-3h. These results have led to operational use of COTREC QPF 0-1h, 1-2h and 2-3h as an operational input into hydrological model HYDROG since spring 2007.

IV. AKNOWLEDGMENTS

This research was supported by the Czech Republic Ministry of Education through grant 1P05ME748.

V. REFERENCES

ALADIN, 2004: 13th ALADIN workshop on ALADIN applications in very high resolution. CHMI, Prague, 2004, ISBN 80-86690-13-X.

Novák P. 2007: The Czech Hydrometeorological Institute's Severe Storm Nowcasting System. *Atmos. Res.*, 83, 450–457.

Šálek M., Novák, P. Seo, D.J., 2004: Operational application of combined radar and raingauges precipitation estimation at the CHMI. *ERAD Publication Series*, 2, 16-20.

Šálek M., Březková L., Novák P., 2006: The use of radar in hydrological modelling in the Czech Republic - case studies of flash floods. *Natural Hazards and Earth System Sciences*, 6, p. 229-236

Investigation of Large Vertical Depth Cb in India

Terrence W. Krauss[1], Andrey A. Sinkevich[2], Nikoly E. Veremey[2], Yulia A. Dovgaluk[2], Vladimir D.Stepanenko[2]

[1] *Weather Modification Inc., 3802, 20 St. N.Fargo, ND 58102, USA (krausst@telusplanetcom)*
[2] *Voeikov Main Geophysical Observatory, Karbyshev str.7,St.Petersburg, Russia, 194021 (sinkev@email.com)*

I. INTRODUCTION

Investigation of severe storms is of great interest to cloud physics as there are a lot of dangerous atmospheric phenomena which are caused by them. There are a lot of publications which present their characteristics and analyze atmospheric conditions when such storms were observed, see, for example, Dovgaljuk et all., 1997, Krauss and Santos,2004, Sinkevich A.A.,2001, Stepanenko V.D., 1983. Here, we analyze the case study when super large Cb was developing. Radar data, satellite data and numerical simulation were used to study main characteristics of the cloud.

.II. PRESENTATION OF RESEARCH

Development of large Cb was observed in Andhra Pradesh province in India on September 28 2004. Cloud top exceeded 18 km. The atmosphere was extremely unstable and convective available potential energy (CAPE) was equal to 6100 J/kg. Observations of the cloud were carried out during 6 hours and 17 min. The storm development was stimulated by several mergings with feeder clouds. The Cb produced intensive lightning though no hail was registered. Meteosat observations showed that a large anvil had formed at the beginning of observations and existed during all the life cycle of the Cb.

Radar measurements indicate that the duration of the developing stage of the storm was equal to 70 min Fig.1), the mature stage 100 min, and the dissipating stage 150 min. Maximum cloud area (projection to surface level) was equal to 1400 km^2. Maximum velocity of top growth was 16.6 m/s and top descent was -11.1 m/s. Radar reflectivity was relatively small for such a huge storm and did not exceed 44 dBz.

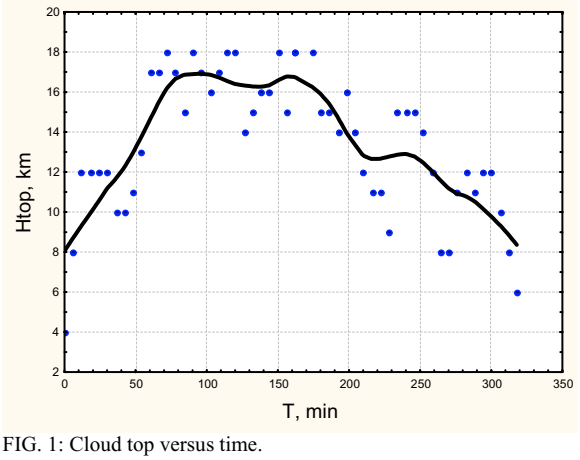

FIG. 1: Cloud top versus time.

Aircraft seeding with AgI glaciogenic reagent to increase precipitation was carried out during 104 minutes. It resulted in significant development of new feeder cells that merged with the main cell and affected the direction of its propagation.

Numerical simulation of storm development was carried out. A 1.5 time dependent numerical model was used. The results had demonstrated that vertical development of the cloud depended on its radius and significant development was observed only for clouds with radius greater than 10 km. Maximum updraft was very big and reached 50 m/s. Maximum LWC was also significant at 7.7 g/m^3.

III. RESULTS AND CONCLUSIONS

Development of a huge tropical storm was observed when the CAPE value was extremely high.

Field experiment and results of numerical modeling indicate that the process of development of this huge tropical storm was determined in great extent by processes of main cell merging with feeder cells. Radar measurements indicate that its reflectivity was relatively small and that is significantly less than one can expect from such a large cloud. The reason could be the result of the absence of hail (no hail was registered from this storm). One can propose that the main mechanism of precipitation formation involved liquid drops coalescence. The formation of ice crystals could be the result of splinters emission during drop freezing. High velocities of updrafts provided possibility for liquid drops to reach high heights where they froze and formed a high concentration of splinters. The high concentration of such ice splinters could possibly be the reason for the absence of hail formation.

Aircraft seeding of the Cb resulted in the formation of new radar echo associated with new precipitation region (feeder cell), and further merging of this new feeder cell with the main cell. All this led to further cloud development.

IV. AKNOWLEDGMENTS

The report was prepared under financial support of Russian Fund of Basic Research and based on the data obtained by WMI in India..

V. REFERENCES

Krauss, T.W., J.R. Santos.,2004: Exploratory Analysis of the Effect of Hail Suppression Operations on Precipitation in Alberta. *Atmos. Res.*, 71, 35-50.

Dovgaljuk Yu.A., et all., 1997: Results of Investigations of Cu cong Characteristics After Seeding. *Meteorology and Hydrology*, 11, .20-29.

Sinkevich A.A.,2001:Cu of North-West of Russia. *Hydrometeoizdat*, 106 p.

Stepanenko V.D., 1983: Radars in Meteorology. *Hydrometeoizdat*, 203 p.

The European Weather Radar Network (OPERA)

Iwan Holleman[1] and Laurent Delobbe[2]
[1]*Royal Netherlands Meteorological Institute (KNMI), Postbus 201, 3730 AE De Bilt, The Netherlands, iwan.holleman@knmi.nl and*
[2]*Royal Meteorological Institute of Belgium (RMI), Av. Circulaire 3, B-1180 Brussels, Belgium, laurent.delobbe@oma.be*
(Dated: April 16, 2007)

I. INTRODUCTION

The OPERA programme (Operational Programme for the Exchange of weather RAdar information, www.eumetnet.eu.org) is the Weather Radar programme of EUMETNET, the Network of the European Meteorological Services (NMSs). The objective of OPERA is to harmonize and improve the operational exchange of weather radar information between national meteorological services. The third phase of the OPERA programme is a joint effort of 28 European countries, runs from 2007 till 2011, and is managed by KNMI. OPERA III is designed to firmly establish the Programme as the host of the European Weather Radar Network. This network currently includes close to 160 operational radars, among which some 110 are Doppler radars (Fig. 1).

The first OPERA programme (1999-2003) put emphasis on the specification of the meteorological products to exchange, to their exchange format, as well as on the software to enable the data exchange. The second OPERA programme (2004-2006) built on these achievements. Its main goal was to increase the exchange and use of the weather radar data in Europe, and to produce a set of recommendations and algorithms for the production of high quality weather radar data, including both wind and precipitation products. A pilot of an European datahub for weather radar data was established at the UK Met Office during this programme (Fig. 2).

FIG. 1: Weather radars in OPERA and EUMETNET member countries. The map is based on entries stored at the OPERA public data base in January 2007.

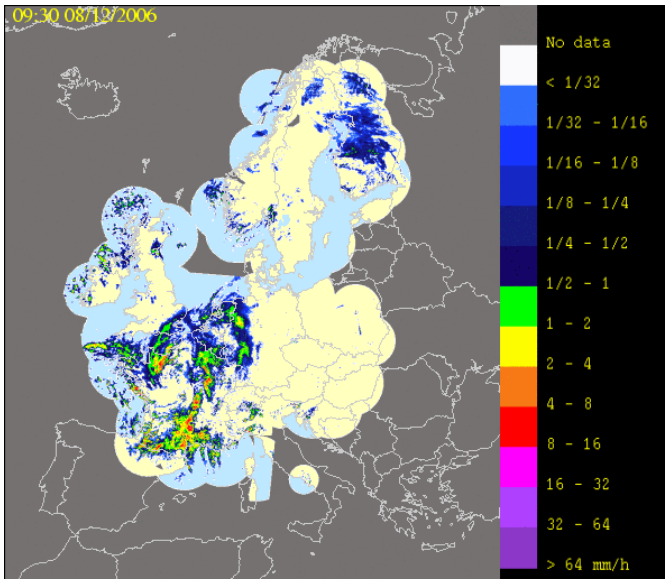

FIG. 2: Example of European composite generated at the OPERA pilot datahub hosted by the UK Met Office.

II. OBJECTIVES OF OPERA III

The fundamental objective of the third phase of OPERA is to provide a European platform wherein expertise on operationally-oriented weather radar issues is exchanged and holistic management procedures are optimized. With the establishment of its Data Hub, OPERA is now organized to support the application of radar data from the European Weather Radar Network. Another important objective of OPERA is to act to harmonize data and product exchange at the European level.

III. MAIN TASKS

The new OPERA programme will focus on the operational generation and quality control of an European weather radar composite, exchange of three-dimensional radar reflectivity and wind data, exchange of quality information, and availability of radar data for official duties of NMSs and research. More specifically, the following tasks are plannned :

1. To maintain an inventory on European weather radars, their characteristics, their data, and products derived from them.
2. To elaborate previous work devoted to understanding and describing radar data quality, in support of their increased quantitative use.
3. To actively provide a forum wherein data providers and users together will define how best to optimize data management procedures.
4. To stimulate the increased exchange and harmonization of weather radar data and products throughout Europe.
5. To support European applications of weather radar data through the establishment of a Data Hub function where harmonized products from the European Weather Radar Network are generated and managed.
6. To investigate and evaluate new radar technology and its relevance to operational requirements for present and future radar systems and products.
7. To provide a forum for information exchange to assist the national protection of radar sites and frequency bands.
8. To maintain support for operational encoding and decoding of radar data and products.
9. To liaise with international organizations (WMO, COST, EUCOS and other EUMETNET Programmes, EUMETSAT, ESA).
10. To inform the meteorological, hydrological, and other operational user communities of its activities.

IV. CONCLUDING REMARKS

Severe storm experts and forecasters are undoubtedly intensive users of weather radar observations and are as such highly concerned by the advances in operational radar meteorology at European level. Operational requirements formulated by the user communities are essential for the radar data providers to increase the quality of their radar data and products. Therefore, the promotion of regular contacts between radar data providers and user communities is one the objectives of the third OPERA programme. More information on the programme can be found on the OPERA website http://www.knmi.nl/opera.

V. AKNOWLEDGMENTS

The authors are endebted to all participants of the OPERA programme who provided material which has been used in this contribution.

CASE STUDY OF A TORNADIC SUPERCELL IN FINLAND 28 AUGUST 2005

Kaisa Outinen, Jenni Teittinen

Finnish Meteorological Institute, Finland, kaisa.outinen@fmi.fi

(Dated: 30 April, 2007)

I. INTRODUCTION

During the morning and before noon hours of 28 August 2005, a supercell thundestorm developed in a surface trough over Gulf of Finland and moved over the Helsinki metropolitan area. The supercell storm produced two successive tornadoes, classified as weak (F1). The second tornado hit a golf course where several people were injured.

The storm travelled trough Helsinki Testbed mesoscale observational network (Saltikoff et al. 2005) and the second tornado occurred near two weather radars (Fig. 1). The storm passed the Vaisala dual polarization Doppler radar at Helsinki University (Kumpula radar) within 5 km and Finnish Meteorological Institute`s (FMI) C-band Doppler radar (Vantaa radar) within few kilometers. Supercell and tornado indicators like hook echo, bounded weak echo region (BWER) and tornado vortex signature (TVS) were discovered in radar images. Hydrometeor types were classified by using differential reflectivity (ZDR).

A few tornadic supercell thunderstorms have been documented in Finland earlier (Teittinen et al. 2006) but they typically seem to occur in the afternoon or evening. Similarly the diurnal tornado peak in Finland is in the afternoon and early evening (Teittinen and Brooks 2006) with less than 10% of cases (mostly waterspouts) occurring before noon. The possibility of a supercell thunderstorm or a tornado was not anticipated by FMI forecasters, so a severe thunderstorm warning was not issued.

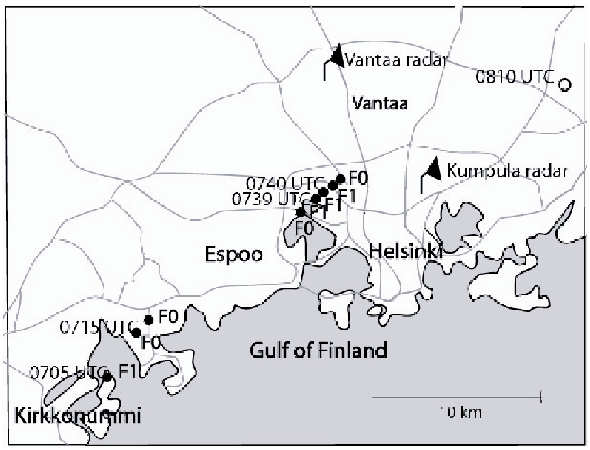

FIG. 1. The location of tornado damage is indicated by black dots with Fujita-scale ratings to each point were damage survey was done. Tornado occurrence times, approximated by the eyewitness observation and emergency reports and locations of two radars has also been denoted.

II. THE STORM ENVIRONMENT

During 28 August 2005, the eastern North Atlantic, Scandinavia and Finland were part of a vast low pressure area (Fig. 2). At night, a wave developed along with 500-hPa trough in southern Sweden and moved northeast toward the Gulf of Finland. The tornadic storm developed at the warm side of the warm front. A low level jet at 850 hPa stretched from the Baltic Sea to the Gulf of Finland and was strengthening and increasing the low-level wind shear during the tornadogenesis. According to Helsinki Testbed mesonet observations, the surface winds were southwesterly before and after the storm. The 300-hPa upper-level jet over southern Finland was weak with maximum wind speeds around 30 m/s.

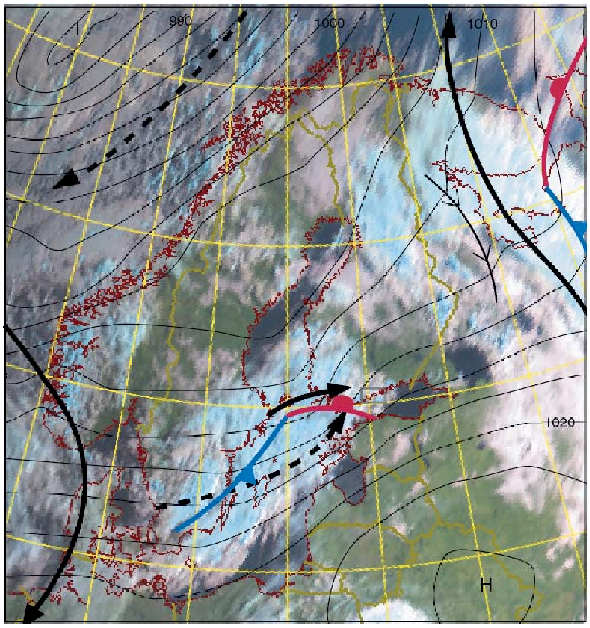

FIG. 2. The ECMWF model analysis of 300-hPa jet axis (solid arrows ≥30 m/s) and 850-hPa low level jet axis (dashed arrows ≥15 m/s) and surface isobars (black lines) overlaid on Meteosat satellite image with manual frontal analysis at 0600 UTC 28 August 2005. The location of Fig. 1 is indicated by grey box.

III. POLARIMETRIC RADAR OBSERVATIONS

The tornadic storm produced two successive tornadoes. The storm first developed over Gulf of Finland. Initially, the radar images showed at 0615 UTC several isolated convective cells, which collided at 0630 UTC when the storm reached the shoreline. The storm developed fast, and moved northeast at an average of 10 m/s. As a signature of a supercell, a hook echo was observed for the first time at 0650 UTC. The first tornado was observed 15 minutes later at 0705 UTC and it lasted for 10 minutes. Based on the damage reports, the tornado was situated at the tip of the hook. The hook echo was evident throughout the storm's whole tornadic phase, until 0810 UTC. At the time the first tornado developed, the storm diameter was 12 km with a height of 6 km, defined by 15 dBZ reflectivity. The maximum reflectivity throughout the storm volume was 57 dBZ at 2 km height. A bounded weak echo region (BWER) was not detected during the first tornado.

The first observation of the second tornado was 20 minutes after the first one, at about 0735 UTC. As the storm had just passed the end of the damage track, a BWER was clearly observed at 0750 UTC (Fig. 3). The BWER with 600 m diameter, was visible at 1 km height with 62 dBZ reflectivity maximum right above BWER at 2.5 km. After the second tornado, BWER was still detectable at 0800 UTC but disappeared after that. One wind damage report was received along the storm track later, at 0810 UTC, thus the storm might have produced third short lived tornado or downburst. The tornado debris cloud is visible in Vantaa radar images (Fig. 4) as reflectivity maximums in the tip of the hook echo. The reflectivity maximums are visible at 300 and 400 m at height with 0.9 and 1 km diameters. During that time the tornado was confirmed at ground and caused F1-damage.

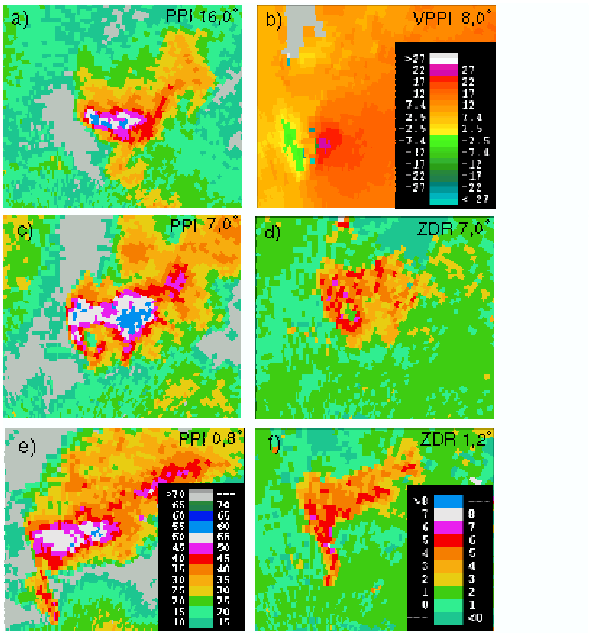

FIG. 3. Kumpula radar a) PPI at 16.0° elevation at 0753 UTC, b) VPPI at 8.0° elevation at 0749 UTC c) PPI and d) ZDR at 7.0° elevation at 0752 UTC, e) PPI at 0.8° elevation at 0750 UTC and f) ZDR at 1,2° elevation 0752 UTC.

The BWER can be also seen in differential reflectivity (ZDR) (Fig. 3d-3f). BWER is formed as a strong updraft carries hydrometeors to higher levels. In the strong updraft, the smallest particles follow the flow and advect back to the cloud. Biggest particles fall against strong updraft and organize around it following the circulation (Dowell et al. 2005). In Fig. 3d, high ZDR values in high reflectivity area around BWER and on the storm left flank suggest massive particles with flattened shapes. Similar ZDR observations have been done in Oklahoma tornadic supercell case (Ryzhkov et al. 2005). High ZDR values dominate throughout the most of the storm, and when coincident with high radar reflectivity, suggest that graupel or hail were not associated with this storm, instead heavy rain. Observations from hail was not received, which supports this assumption.

Mesocyclone signature is shown in Doppler velocity data in Fig. 3b. Highest tangential velocity in mesocyclone was ±15 m/s. Diameter of mesocyclone at 0749 UTC was about 1.5 km at 900 m height. The tornado vortex signature (TVS) had 300 m diameter at 300 m height, and differential velocity of 18 m/s and was situated right rear edge of the mesocyclone core.

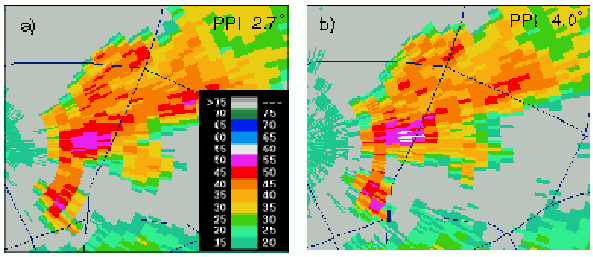

FIG. 4. PPI of reflectivity from Vantaa radar at a) 2,7° elevation at 0749 UTC and b) 4,0° elevation at 0747 UTC. The debris cloud range from the radar is 4 km.

IV. DISCUSSION

The Finnish Meteorological Institute did not issue warning for this tornadic supercell. The forecasters don't have in operational use tools like radar algorithms to help to detect potentially severe storms from general thunderstorms and the warning area covers the whole Finland. In operational radar pictures this small storm did not appear to be severe. Also the time of the event was unusual, since tornadoes in Finland typically occur in afternoon and early evening. This study has shown that the severe thunderstorm signs were detectable well before the tornadogenesis. If similar storms want to be warned for in the future, the operational radar tools have to be developed further.

V. ACKNOWLEDGEMENTS

The authors would like to thank David M. Schultz for the his comments during the preparation of the abstract. The authors thank Harri Hohti for his help with processing the radar data.

VI. REFERENCES

Dowell D. C., Alexander C. R., Wurman J. A., Wicker L. J., 2005: Centrifuging of Hydrometeors and Debris in Tornadoes: Radar-Reflectivity Patterns and Wind-Measurement errors. *Mon. Wea. Rev.*, 133, 1501-1523.

Ryzhkov A. V., Schuur T. J., Burgess D. J., 2005: Polarimetric Tornado Detection. *Journal_of applied meteorology,* 44 , 557-570.

Saltikoff E., Dabberdt W. F., Poutiainen J., Koistinen J., Turtiainen H., 2005: The Helsinki Testbed: A four-season mesoscale research and development facility. Preprints, *13th Symposium on meteorological observations and instrumentation.* Amer. Meteor. Soc., CD-ROM

Teittinen J., Brooks H. E., 2006: A climatology of tornadoes in Finland. Preprints, *23rd Conference on Severe Local Storms*, St Louis, Amer. Meteor. Soc., CD-ROM.

Teittinen J., LaDue J., Hohti H., Brown R. A., 2006: Analysis of a tornadic mini-supercell in Finland by using Doppler radar. Preprints, *23rd Conference on Severe Local Storms*, St Louis, Amer. Meteor. Soc., CD-ROM.

Study on the Mesoscale Structure of Heavy Rainfall on Meiyu Front with Dual-Doppler Radar

Zhou Haiguang

State Key Laboratory of Severe Weather, Chinese Academy of Meteorological Science, Beijing 100081, China, zhg@cams.cma.gov.cn

(Dated: September 12, 2007)

I. INTRODUCTION

Dual-Doppler radar wind retrieve technology can improve the accuracy of the three dimensional wind fields. Armijo (1969) studied the wind synthesize method with dual-Doppler radar firstly. Many new retrieve methods were proposed in recent years (Bousquet and Chong, 1998; Shapiro and Mewes, 1999; Chong and Bousquet, 2001). It is an important way to study the 3D structure of the heavy rainfall, hail and squall line et al (Jeffrey et al, 2006; Kropfli and Miller, 1976; Parsons, et al, 1987; Smull and Houze, 1987; Zhou and Wang 2005; Zhou and Zhang, 2005;).

II. PRESENTATION OF RESEARCH

The dual-Doppler radar network is composed by the radars located in Hefei and Maanshan city in South China. Due to the effect of the convergence line and the mesoscale convection system, it produced a heavy precipitation in the dual- Doppler coverage area between 26th and 27th June 2003. The heavy rainfall is 108.1mm in Quanjiao city from 2200 LST to 2400 LST on 26th.

The 3D wind fields are retrieved by MUSCAT method using the dual-Doppler volume scan data. This method is proposed by Bousquet and Chong (1998). Zhou and Zhang (2002) use it to retrieve the ground-based dual-Doppler 3D wind.

By 2050 LST 26 June, some cells had begun to develop at the east of Hefei city. These cells developed and combined very quickly. After one hour, a mesoscale band echo system extended from southwest to northeast near Caohu and Quanjiao city and propagated eastward. The peak reflectivity is greater than 45dBZ. The heavy rainfall occurred after the band formed. The band system lasted for more than 2 hours. The high reflectivity core in the band began to decrease after 2400 LST. At the same time, the rainfall began to weak.

The retrieve wind by dual-Doppler radar on 2107 LST shown that the retrieve area was contraled by southwest wind. By 2151 LST, the convergence line formed at 1.5km AGL. By 2202 LST, the convergence line is more stronger than the former time and propagated to the upper levels. The higher-reflectivity band was corresponded to the convergence line. It indicated that the wind field is the kinematic foundation of the reflectivity field evolution.

Fig. 1 showed the wind fields on 2235 LST. There are strong convergence line at the low and middle level (1.5~4.5km AGL) which are more clear than former time, but the convergence line is weak at the middle level. The upper level above 5km AGL were controlled by southwest air flow. There was strong reflectivity on the low and middle level near Quanjiao.

Fig. 2 showed the velocity of the vertical cross section along x=69km. There are strong updrafts near the convergence area. The flow at the low level formed the inflow and the flow at the upper low in the north area is the outflow region which moved northward. Strong precipitation was occurred in the updraft with high reflectivity. There was a strong cell near Quanjiao city. This configuration was an important mechanism for the initiation and maintain of the heavy rainfall.

This configuration lasted for more than 2 hours which caused the heavy rainfall on 2200~2400 LST, up to 108.1mm in Quanjiao.

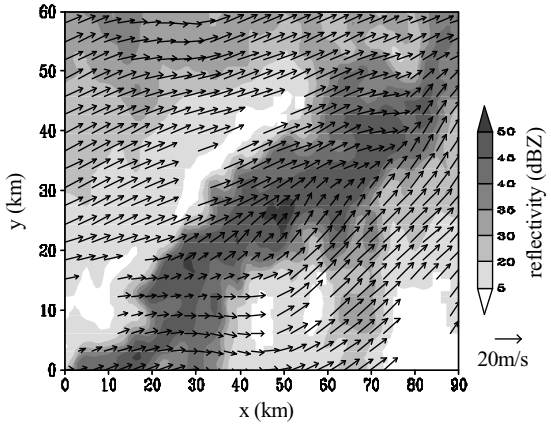

FIG. 1: Horizontal wind at height of z=1.5km AGL on 2235 LST

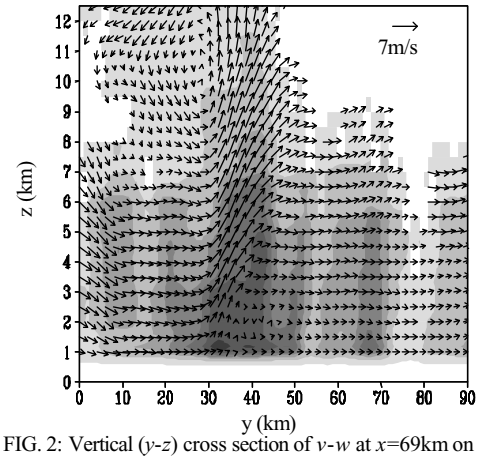

FIG. 2: Vertical (y-z) cross section of v-w at x=69km on 2235 LST

After 2337 LST, the local storm began to weak, and the reflectivity near the convergence line decreased while high reflectivity was still strong at the low level of Quanjiao. The convergence line at the low and middle level was still maintained. This shown that the local rainfall will last. By 0125 LST 27th, the high-reflectivity cells at the low and middle level were more weaken while the rainfall was weak. In the vertical cross section, the flow at the middle and upper level is smooth and weak. All these details showed that this storm would dissipate.

III. RESULTS AND CONCLUSIONS

In this, the three-dimensional wind fields of the heavy rainfall on the Meiyu front were retrieves and studied that occurred on 26th-27th June 2003 in Huaihe river basin, using the volume scan data of the dual-Doppler radar located in Hefei and Maanshan cities. The mesoscale convective system (MCS) and the cells located on the MCS play important role on this heavy rainfall. The wind retrieval showed that this heavy rainfall was caused by the mesoscale convergence line at the low and the middle level which triggered and maintained the heavy rain. There are strong convergence and vorticity at the lower and middle layer of the MCS. The three-dimensional kinematic structure model was also given and discussed.

IV. AKNOWLEDGMENTS

This research was supported by the National Science Foundation of China through Grant 40605014 and the National Key Basic Research and Development Project of China-research on theories and methods of monitoring and predicting of heavy rainfall in South China through Grant 2004CB418300.

V. REFERENCES

Armijo L.,1969: A Theory for the Determination of Wind and Precipitation Velocities with Doppler Radar. *J. Atmos. Sci.*, 3 570-573.

Bousquet O., Chong M.,1998: A Multiple-Doppler Synthesis and Continuity Adjustment Technique (MUSCAT) to Recover Wind Components from Doppler Radar Measurement. *J. Atmos. Oceanic Technol.*, 13 343-359.

Chong M., Bousquet O., 2001: On the Applicaton of MUSCAT to a Ground-Based Dual-Doppler Radar System. *Mete. Atmos. phys.*, 78 133-139.

Jeffrey R. B., John L. S., Wurman J. M., 2006:High-Resolution Dual-Doppler Analyses of the 29 May 2001 Kress, Texas, Cyclic Suppercell. *Mon. Wea. Review*, 134 3125-3148.

Kropfli R. A., Miller L. J., 1976: Kinematic Structure and Flux Quantities in a Convective Storm From Dual-Doppler Radar Observations. *J. Atmos. Sci.*, 3 20-29.

Parsons D. B., Mohr C. G., Gal-Chen T., 1987: A Severe Frontal Rainband. Part III: Derived Thermodynamic Structure. *J Atmos. Sci.*, 44 1621-1631.

Shapiro A, Mewes J. J., 1999: New Formulation of Dual -Doppler Wind Analysis. *J. Atmos. Oceanic Technol.*, 16 782-792.

Smull B. F., Houze R. A., 1987: Dual-Doppler Radar Analysis of a Midlatitude Squall Line with a Trailing Region of Stratiform Rain. *J. Atmos. Sci.*, 44 2128-2148

Zhou H. G., Zhang P. Y., 2002: A New Technique of Recovering Three-Dimensional Wind Fields From Simulated Dual-Doppler Radar in the Cartesian Space. *Acta Meteorologic Sinica,* (In Chinese), 60 585-593.

Zhou H. G., Wang Y. B., 2005: Structure of Meso-ß and –?-Scale on Meiyu in Huaihe River Basin on 30 June, 2003 by Dual-Doppler Radar. *Acta Meteorologic Sinica,* (In Chinese), 63 301-312.

Zhou H. G., Zhang P. Y., 2005: Study on the 3-D Wind of Heavy Rain with Dual-Doppler Radar. *Chinese Journal of Atmospheric Science* (In Chinese), 29 372-386.

RAIN EVENT ON 22 OCTOBER 2006 IN LEÓN (SPAIN): DROP SIZE SPECTRA

María Fernández-Raga, Amaya Castro, Covadonga Palencia, Ana I. Calvo, Roberto Fraile

Universidad de León, Facultad de CC Biológicas y Ambientales, 24071 León, Spain
mferr@unileon.es, rfral@unileon.es
(Dated: April 27, 2007)

I. INTRODUCTION

Size spectra of hydrometeors such as raindrops or hailstones are essential in many research projects. Remote detection of rain by radar, for example, is parametrized by the reflectivity factor, which depends on the number of raindrops and their size distribution (Berenguer et al., 2005). Soil erosion through the impact of rain depends on the kinetic energy of the drops, which is also a function of their size (Cerro et al., 1998).

This study describes the physical characteristics of precipitation on the wettest day of the year 2006 in León, Spain. The aim is to analyze the atmospheric situation during 24 hours by means of various techniques (synoptic situation, satellite imagery, radio sounding, rain gauge and disdrometer), and finding relationships between the most representative variables.

This is one single instance that continuous previous studies (Fraile et al., 2005) on the temporal sequencing of precipitation processes, and this study presents the methodology followed to identify patterns in the evolution of the precipitation.

II. METEOROLOGICAL SITUATION

Fig. 1 shows the synoptic map on the surface and at 500 hPa. It can be seen that around the Iberian Peninsula the meteorological situation is characterized by the presence of a large trough whose leaving zone is located right over the Iberian Peninsula. These are ideal conditions for instability. 24 hours later the trough deepened still further and came closer to the study zone.

Nevertheless, the radio soundings carried out near the study zone show a low level of instability (CAPE was nearly zero). The radar imagery shows the cloud layer over León that day causing the highest daily precipitation registered in 2006.

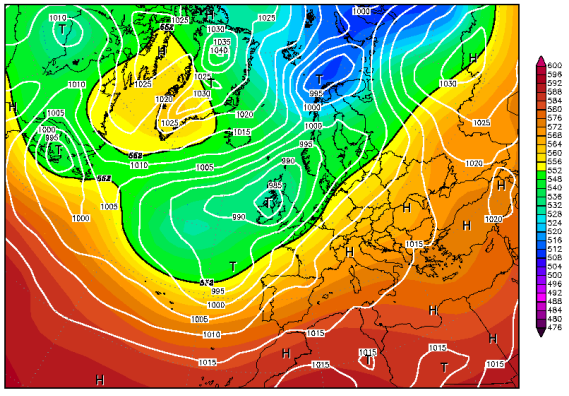

FIG. 1: Meteorological situation on 22nd October 2006 at 0000 GMT on the surface and at 500 hPa (courtesy of Wetterzentrale).

The Spanish Instituto Nacional de Meteorología provided images from a radar located at approximately 80 km from the study zone. The images show different cloud formations constantly crossing the sky over León, although at moderate reflectivity factors.

The result of this meteorological situation is summarized in Fig 2, which represents the total precipitation registered minute by minute in the city of León from 0000 GMT on the 22nd until 0000 GMT on the 23rd. Rain fell continually during the whole day, with two moments of particular intensity (from 1100 to 1140, and from 2225 to 2350 GMT).

III. RESULTS AND CONCLUSIONS

The optical disdrometer used in the city of León uses data on drop size and integrates them in intervals of one minute each. We have employed the transformations found by Brandes et al. (2002) and Park et al. (2005) to calculate the volume of a rain drop from its maximum diameter on the horizontal. It is thus possible to represent the intensity of the precipitation in each minute (it is similar to the derivative of the curve in Fig. 2). This intensity (with a better resolution than the curve in Fig. 2) is represented in Fig 3. In Fig. 3 we can see the two most intense precipitation events: the first, from 1100 GMT on, exceeded 25 mm/h; the second, around 2300 GMT nearly reached 40 mm/h.

Fig. 4 shows the size histogram of the rain drops registered during the whole day. The disdrometer registered nearly 10^6 drops in these 24 hours. The distribution can be seen to be approximately exponential, with very many small drops and very few large drops (only 3 drops of over 5 mm were registered, and they are not included in Fig 4). The parameter of the exponential is 2.75 mm^{-1}.

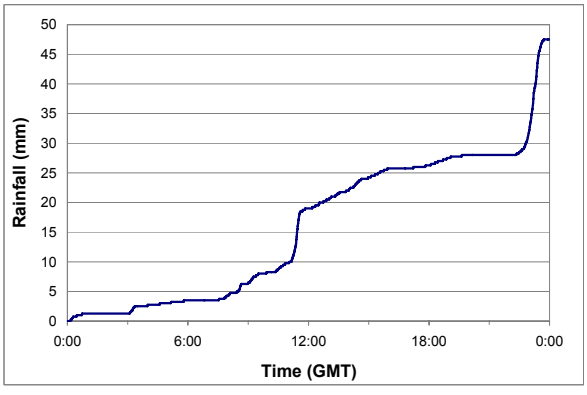

FIG. 2: Evolution of the total amount of precipitation registered.

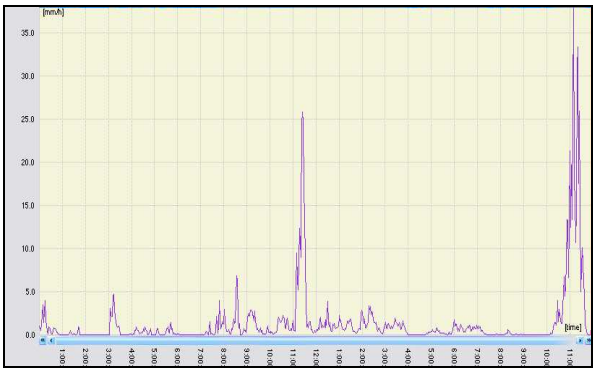

FIG. 3: Rain intensity during the 22nd October 2006.

The distribution does not remain constant during the day. Fig. 5 shows the temporal evolution (every five minutes) of the size spectrum in the two most intense moments mentioned above. There are variations in the total number of drops as well as in the size spectrum.

IV. ACKNOWLEDGMENTS

The authors are grateful to Dr. Noelia Ramón for translating the paper into English. We would also like to thank the Spanish Instituto Nacional de Meteorología and Wetterzentrale for providing the data used in this paper.
We are also indebted to Antonio M. Ortín, Toyi del Canto and Julio Otero for their technical assistance, and to Juan Pablo Älvarez and Nieves Garrido for their helpful suggestions.

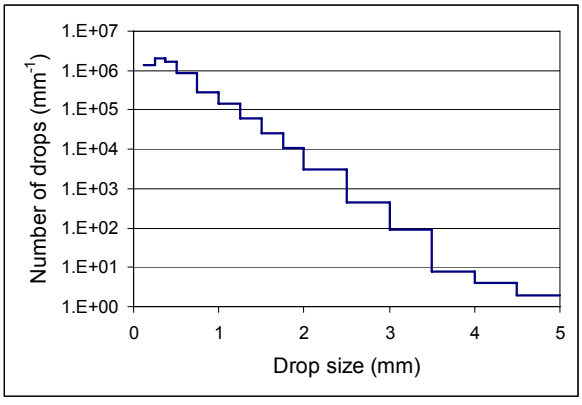

FIG. 4: Size spectrum of the drops registered during the whole day.

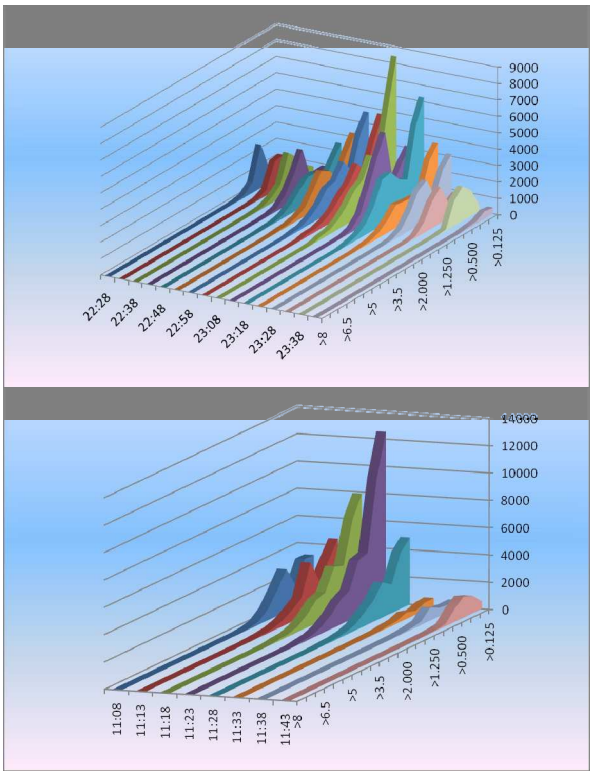

FIG. 5: Evolution of the size spectrum.

V. REFERENCES

Berenguer M., Corral C., Sánchez-Diezma R., Sempere-Torres D., 2005: Hydrological validation of a radar-based nowcasting technique. *J. Hydrometeor.,* 6 532-549.

Brandes E. A., Zhang G., Vivekanandan J., 2002: Experiments in rainfall estimation with a polarimetric radar in a subtropical environment. *J. Appl. Meteor.,* 41 674–685.

Cerro C., Bech J., Codina B., Lorente J., 1997: Modeling rain erosivity using disdrometric techniques. *Soil Sci. Soc. Amer. J.*, 62 731-735.

Fraile R., Fernández-Raga M., Montero-Martínez G., Castro A., García-García F., 2005: Evolución temporal de la precipitación en los episodios de lluvia de León (España). *XI Congreso Latinoamericano e Ibérico de Meteorología,* Cancún.

Park S., Bringi V., Chandrasekar V., Maki M., Iwanami K., 2005: Correction of radar reflectivity and differential reflectivity for rain attenuation at X-band, Part I: Theoretical and empirical basis. *J. Atmos. Ocean. Technol.*, 22 1621-1632.

DISCRIMINANT ANALYSIS APPLIED ONTO HAIL DETECTION USING RADAR

López L., Sánchez J.L., García-Ortega E. and Marcos J. L.,

Laboratory of Atmospheric Physics, University of León, Spain, llopc@unileon.es

(Dated: April 20, 2007)

I. INTRODUCTION

There are a number of tools available – and more are currently being developed — to discriminate, within a particular storm, areas with hail precipitation using data provided by conventional meteorological radar systems (Waldvogel and Federer, 1979; Greene and Clark, 1972; Rasmussen and Wilhelmson, 1983; Kizmiller and Breindenbach, 1993; Witt et al., 1998). However, at a supraregional level most of the methods that have traditionally been employed to identify hailstorms often present ambiguous results. (Edward and Thompson, 1998). Caution is required when it comes to extrapolate the various identification models to areas other than the ones where they were developed.

On the other hand, many currently available systems for data extraction and treatment make it relatively easy to obtain a large number of variables derived from radar parameters for each storm analyzed and at different stages in its development. The questions are now: is it possible to select and/or classify these variables according to their ability to discriminate hailstorms from non-hail storms? And if so, would the combination of several of these variables enable us to develop new and improved discriminating tools? These issues have taken us to the *stepwise* method used to develop radar-based hail–detection-products implemented in the northeast of the Iberian Peninsula.

II. STUDY ZONE

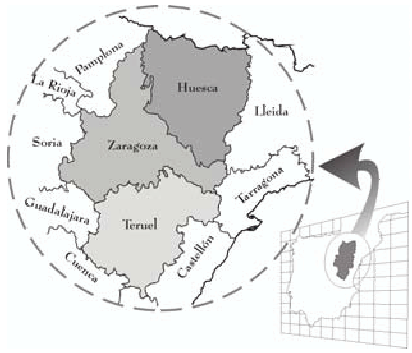

FIG. 1: Study zone.

The study zone (Fig. 1) lies in the northeast of the Iberian Peninsula, more precisely in the Valley of the River Ebro. It comprises nearly the whole of the Region of Aragón and part of the province of Lérida (about 40 kilometers of the area known as *Ponent de Lleida*).

This zone lies between 39º 51´ and 42º 55´ N, and 2º 06´ W - 0º 44´ E.

The region has an important convective activity, and the radar imagery shows that there are approximately 60 storm days every summer. The damages caused by hailstorms in the study zone amount annually to about 100 M€, which indicates the relatively high frequency of this phenomenon and their important economic impact.

The *Laboratory of Atmospheric Physics* at the University of León, Spain, owns a portable C-band radar which was installed in the study zone to gather data during the experimental campaign. The radar was set up 10 km SW of the city of Zaragoza, and its range was estimated at a radius of 140 km from that point. TITAN Software *(Thunderstorm, Identification, Tracking, Analysis and Nowcasting)* was used, providing data for a pixel size of 1 km, both horizontally and vertically.

With respect to the methodology employed, whenever a particular storm cell was seen to reach a maximum reflectivity of 35 dBZ or more, the local observer was phoned up to determine the type of precipitation registered on the ground, thus distinguishing between rain and hail. For this study a total of 729 towns and villages were included all over the study zone, and there was at least one meteorological informer in each.

The methodology described above provided a database of the *ground truth.* All in all, a radar image and the corresponding ground truth of 702 instances were gathered, 308 of which corresponded to hail precipitation and 394 to rain, according to the information provided by the *in situ* observers.

III. METHODOLOGY AND RESULTS

In discriminant analyses it is convenient that the independent variables fulfill a number of preliminary conditions: normality, linearity and multicollinearity. In addition, the model must comply with the assumption of homoscedasticity, and the population means of the two groups must differ significantly (Hair, 1999). Once these preliminary conditions had been noticed, the independent variables were selected that would lead to the most powerful and stable estimation possible.

The aim was to select the most appropriate variables to discriminate hail tracks from non-hail tracks, and the *stepwise* method was employed (Carrasco and Hernán, 1993). With this

method the independent variables are introduced one by one in a discriminant function according to their discriminating power.

The whole sample of tracks was arbitrarily divided into two parts in order to set up the model. One part of the sample – formed by 276 non-hail track and 202 hail tracks - was used to set up the discriminant equation, and the remaining third of the total sample was later used to validate the results.

To control the stepwise introduction of the variables, the Squared Mahalanobis Distance was used. The minimum threshold value was established at 0.01, and the value 0.1 was established for eliminating variables (Hair, 1999). In each one of the iterations in the analysis the Wilks *lambda* decreased from 0.423 to 0.369 in the last step. The Fisher-Snedecor *F* statistic shows that these changes were significant in all the steps.

In the end, six variables fulfilled the minimum criteria to be considered significant discriminators on the basis of their Wilks *lambda* and the minimum values of Mahalanobis D^2.

The six variables selected (Altitude of maximum reflectivity, D dBZ max/dt, Top, Square root of VIL, Square root of the maximum reflectivity and Square root of the inclination) were included in the final discriminant function. The total variance explained by the discriminant function is 0.632 (Hair, 1999), and the function obtained shows a canonical correlation value of 0.795.

It must be taken into account that the chances of belonging to the hail group or the non-hail group need not be the same. Because of this, the Fisher's linear discriminant functions calculated for each group considered the various *a priori* possibilities for each of the groups studied.

In order to assess the forecasting power of the discriminant function, contingency tables were calculated for both the main sample and the validation sample. The validation sample consisted of 224 tracks. Finally, different precision indices were calculated to account for the goodness of the forecast.

The probability of detection is 0.923 in the main sample, and 0.868 in the validation sample. Even though the score is somewhat lower in the latter case, as expected, it can still be considered a very satisfactory result. The False Alarm Ratio was very low (0.08 and 0.123, respectively). The frequency of unforeseen events is 0.054, which guarantees that very few events will go undetected.

The results for HSS and TSS are 0.7685 and 0.7679 in the validation sample. The value of these indices lies between –1 and 1, which would correspond to a perfect forecast. It can be seen that the values found point towards a very good performance of our model.

IV. AKNOWLEDGMENTS

The present study has been supported by the CICYT Project SEVERUS (CGL2006-13372-C02-01).

V. REFERENCES

Carrasco, J. L. y M. A. Hernán; 1993: Estadística multivariante en las ciencias de la vida. Editorial Ciencia, Madrid, 347 pp.

Edwards, R. E., y Thompson, R. L., 1998: Nationwide Comparisons of Hail Size with WSR-88D Vertically Integrated Liquid Water and Derived Thermodynamic Sounding Data, *Wea. And Forecasting*, **13**, 277-285.

Greene, D. R., y R.A. Clark, 1972: Vertically integrated liquid-A new analysis tool. *Mon. Wea. Rev*., **100**, 548-552.

Hair J. F., R. E. Anderson, R. L. Tatham, W. C. Black, 1999: Análisis Multivariante. Prentice Hall Iberia. Madrid. 1999

Kitmiller, D. H., y J. P. Breidenbach, 1993: Probabilistic nowcasts of large hail based on volumetric reflectivity and storm environmental characteristics. Preprints, 26th Conf. on Radar Meteorology, Norman, OK, Amer. Meteor. Soc., 157-159

Rasmussen, E.N. y R.B. Wilhelmson, 1983: Relationship between storm characteristics and 1200 GMT hodographs low-level shear and stability. Preprints, 13th Conf. on Severe Local Storms. Tulsa, OK, Amer. Meteor. Soc., J5-J8.

Walvogel, A., Federer, B., and Grimm, P., 1979: Criteria for the Detection os Hail Cells, *J. Appl. Meteor.,* **18**, 1521-1525.

CHARACTERIZATION OF CONVECTIVE RAINFALL USING C-BAND DUAL-POLARIZED RADAR AND MODELS INTERCOMPARISON: COSMO-LAMI AND MM5.

L.Molini[1], K. De Sanctis[2], A.Parodi[1], R. Ferretti[2], F.S. Marzano[3,2], M. Montopoli[4] and F.Siccardi[1]

1 *CIMA-University of Genoa, ITALY, luca.m@cima.unige.it*
2 Department of Physics/CETEMPS, University of L'Aquila, ITALY,rossella.ferretti@aquila.infn.it
3 DIE, University of Roma "La Sapienza", Rome, ITALY,
4 Department of Engineer*/CETEMPS, University of L'Aquila, ITALY*
(Dated: April 30, 2007)

I. INTRODUCTION

In the last few years, the polarimetric upgrading of weather radars has allowed to improve considerably the accuracy related to the estimation of rain rate and to the hydrometeors classification, mainly in deep convective events. Recently, the need to deepen the analyses on such issues has been tackled by means of the development of modelling chains composed by high resolution numerical weather prediction models able to generate atmospheric scenarios with desired characteristics and radar simulation modules feed with the 3-D output fields of the aforementioned atmospheric models.

II. PRESENTATION OF RESEARCH

This work focuses primarily on the evaluation of the effects of different microphysical parameterizations embedded into two atmospheric limited area model (COSMO-MODEL and MM5) on the simulated co-polar and differential reflectivity datasets computed by radar simulation software (RSM). Since the latter is able to provide C-band polarimetric signatures of different hydrometeors, a second important task is constituted by the intercomparison of both simulated and the available observed reflectivity fields so as to assess the reliability of both models in reproducing deep convective weather conditions with a particular attention on the dynamics of the precipitation processes.

III. RESULTS AND CONCLUSIONS

Particularly, a severe event occurred over Northern Italy on 20/05/2003 has been simulated through the above mentioned numerical. The radar simulator allows for better comparing the models products with the radar. The models clearly reproduce the convective cell observed by the two radars, and they are both able to identify the event has a hail storm. Further work will be devoted in analyzing the sensitivity of both models to different microphysical parameterizations while simulated radar data will be compared with real data provided by ARPA-SIM's polarimetric radars of Gattatico and S.Pietro Capofiume.

IV. AKNOWLEDGMENTS

The authors would like to thank ARPA-SIM for LAMI and Radar data, NCAR for MM5.

V. REFERENCES

Alberoni, P. P., Zrnič, D. S., Ryzhkov, A. V., and Guerrieri, L.: Use of a fuzzy logic classification scheme with a C-band polarimetric radar: first results, Proceedings of ERAD, pp. 324–327, 2002.

Haase, G. and Crewell, S. : Simulation of radar reflectivities using a mesoscale weather forecastmodel. Water Resources Research, 36, 2221-2230, 2000.

Marzano F.S., D. Scaranari, M. Celano, P.A. Alberoni, G. Vulpiani, and M. Montopoli: Hydrometeor classification from Dual-Polarized weather Radar: Extending fuzzy logic from S-Band to C-Band data**.** *Advances in Geosciences, 2006.*

Molini L., Assessing radar measurements uncertainty using a high resolution atmospheric/remote sensing modelling chain, Ph.D thesis, 2007.

The statistical characteristics of results of radar observations of atmospheric phenomena related to Cb

Ph.D. Huseynov N., Malikov B.
Enterprise "Azerairnavigation", Int. Airport Heydar Aliev/Baku, Azerbaijan, nazim@azans.az
(Dated: September 14, 2007)

I. INTRODUCTION

The weather phenomena related to Cb impacts on the aviation safety. In this connection the statistical analysis of the radar-tracking data has the significant importance for researching these phenomena in the certain flights region.

The implementation of statistical characteristics of weather phenomena in the radius of 300 km of the aerodrome "Heydar Aliev" (Baku) based on the radar data for the period 2004-2006. The statistical characteristics are based on the following phenomena: frequencies of Cb and storm activity, the top height of the convective clouds with storm and total amount of showers.

II. PRESENTATION OF RESEARCH

The results of statistical analysis of Cb average frequencies for the period of 2004-2006 is indicated in the figure 1.

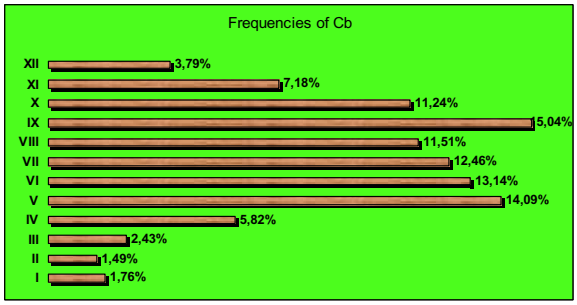

FIG 1. The histogram of the average frequencies of Cb for the period of 2004-2006.

According to the histogram the maximum occurrences of Cb are typical for spring and summer periods.

Statistical research of Cb with storms activities also indicates their advantage occurrence during spring and summer periods (FIG 2).

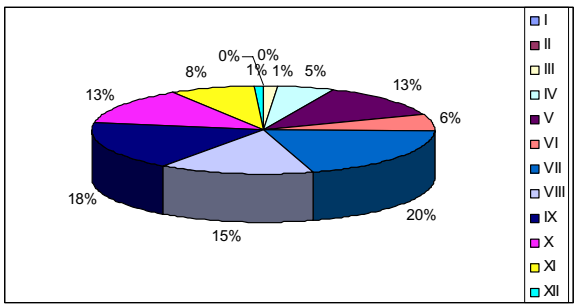

FIG 2. The diagram of storm activities.

The histogram created on the top height of Cb with storm is shown in the figure 3.

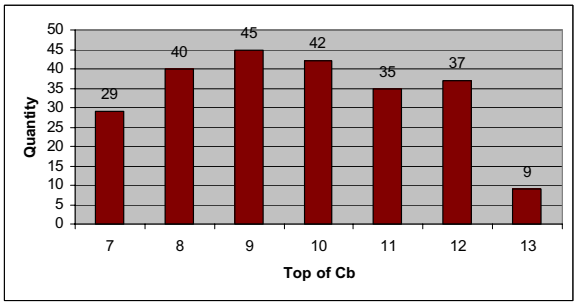

FIG 3. The histogram of the top height of storm clouds.

The highly common altitudes were 8-10 km (55%).

According to the research showers consist 50,2% of all atmospheric precipitation.

III. RESULTS AND CONCLUSION

According to climatic characteristics of Baku storm clouds formation is typical for frontal process, intramass - are observed extremely seldom. In this region storms are being formed under three definite types of synoptic conditions:

1. Most frequently storms are formed in a warm season, when from the side of Caspian sea the cold air masses advect to the middle troposphere in the presence of relatively high pressure of warm air masses above Northern Africa.
2. Storms are also formed during advection of cold air masses when the cold front is passing the region.
3. Within all year particularly in spring season when passing warm fronts with warm air masses may cause favorable conditions for the development of storm clouds.

On the basis of research dependence of storms on top borders of convective clouds has been determined. According to this dependence frequencies of occurred storms show the best correlation with the heights 7-10 and 13 km (FIG. 4).

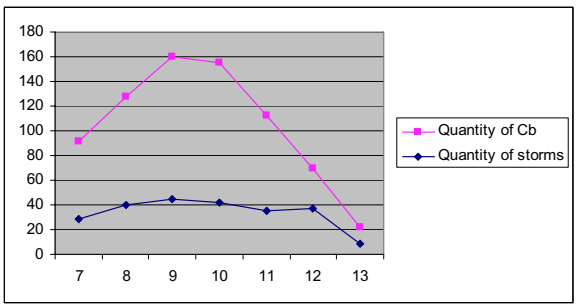

FIG. 4. Dependence of storms on top borders of convective clouds.

IV. REFERENCES

Hans A. Panofsky. University Park Pennsylvania-1958: “Some applications of statistics to meteorology”. pp. 169-171.

Pashayev A.M., Imanov F.A., Huseynov N.Sh., Guliev H.I. 2007: “Climatic characteristic of aiport Heydar Aliev”. pp. 93-95.

Sultanov V.Z., Huseynov N.Sh., Malikov B.M. 2004: “Radar meteorology”. pp. 94-112.

SEASONAL AND INTERNANNUAL VARIATIONS OF INDIAN SUMMER MONSOON WINDS – A STUDY USING INDIAN MST RADAR

M. Roja Raman[1], V.V.M. Jagannadha Rao[2], G. Kishore Kumar[1], A. Narendra Babu[1], M. Venkat Ratnam[3] and S.V.B. Rao[1]

[1]Department of Physics, Sri Venkateswara University, Tirupati – 517 502, India
[2]Department of Physics, S.V. Govt. Polytechnic, Dept of Tech. Education, Tirupati – 517 502, India
[3]National Atmospheric Research Laboratory (NARL), Post box No: 123, Gadanki, Tirupati – 517502, India.

I. INTRODUCTION:

The perspective of possible influence of global climate change on monsoon and its variability remains a major issue of concern for the large population of developing country like India where the agriculture and thus economy is closely linked with the behavior of the monsoons during which most of the annual rainfall occurs.

Precipitation patterns in the Indian sub-continent are characterized by dry conditions in the early summer and relatively moist conditions in late summer. The Indian Summer Monsoon, which is part of a large scale circulation pattern known as the Asian Summer Monsoon, develops in response to the large thermal gradients between the warm Asian continent to the north and cooler Indian Ocean to the south. Indian summer monsoon is characterized by few important features in the troposphere such as seasonal wind reversal in the lower level, upper level Tropical Easterly Jet stream (TEJ) [Reiter, 1961], humidity variations, wind shear etc,. The study of these features is important as they reveal the strength of the monsoon and its variability from year to year. In the past, investigations were carried out on monsoon features with different data sets of Radiosondes [Koteswaram, 1958], which have poor height resolution. Since TEJ is relatively stationary around 15^0 N for few days and the MST Radar site is nearer to 13^0 N it is possible to study its characteristics.

II. PRESENTATION OF RESEARCH

(a) DATA

Using Indian MST Radar with its good vertical height resolution, an attempt has been made first time to study statistically the monsoon characteristics such as Monsoon winds, Tropical Easterly Jet and its variation, and vertical circulation over Gadanki (13.5˚ N; 79.2˚ E) using nearly 9 years of data. Rain gauge data over Gadanki and India meteorological department (IMD) rainfall data over Andhra pradesh is taken to observe the relation with rainfall occurrence and monsoon wind characteristics.

(b) RESULTS AND DISCUSSIONS

Few important features are observed during the evolution and progress of the monsoon. The average depth of westerlies during monsoon period is found to be around 7.8 km. The mean core height of the Tropical Easterly Jet (TEJ) is around 16.2 km. The average jet speed is observed to be 39.2 ms^{-1} and attained values up to 55 ms^{-1} on few individual days.

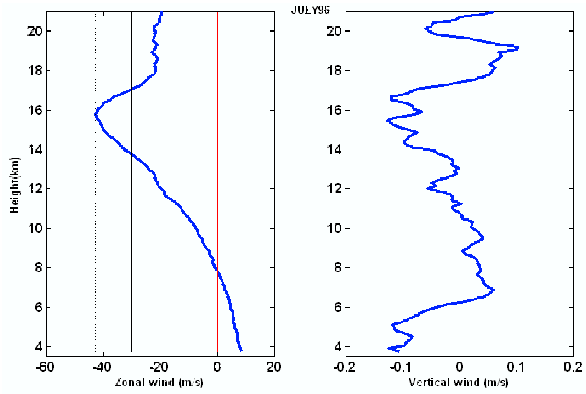

FIG(1): Zonal and vertical wind variations during Monsoon season

The profiles of monthly mean vertical velocity show direction reversal from downward to upward at two regions, one around zonal wind reversal height and another at around jet core height (fig 1). The mechanism of this vertical velocity reversal is thought to be due to horizontal convergence and instabilities associated with the jet streams respectively. Similar feature was noted by Jagannadha Rao et al (2001) with 3 years of data set using Indian MST Radar. The mean meridional winds, although magnitudes are small, show northward motion above and southward motion below jet core height. The vertical wind shear above jet core height is observed to be greater than below jet core height. Daily accumulated rainfall data over observation site and IMD rainfall data over Andhra Pradesh state are compared with the variation of wind reversal height during monsoon season. Here it is observed that there is a negative correlation between the rainfall

occurrence and wind reversal height (Fig 2), which shows that as the wind reversal height is more the rainfall is less and vice versa. Further study is being carried out to observe weather the correlation is same through out the country or not.

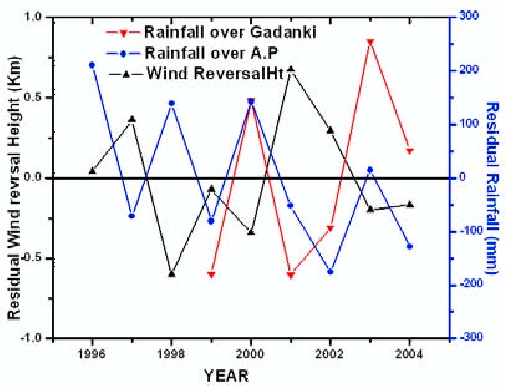

FIG (2): The Correlation between rainfall and wind reversal height.

III. AKNOWLEDGMENTS

The authors wish to thank National Atmospheric Research Laboratory (NARL) and ACAS, S.V. University, Tirupati for providing data and necessary facilities to carry out this work. We are thankful to India Meteorological Department for providing radiosonde data. V.V.M.J. Rao is thankful to The Commissioner, Department of Technical Education, Government of Andhra Pradesh for permitting him to carry out this research. M.R.R is thankful to ISRO for providing JRF to carry out this work.

V. REFERENCES

1. Koteswaram, P., 1958: The easterly jet stream in the Tropics. *Tellus* 10**,** 43–57.

2.Asnani, G. C., 1993: *Tropical Meteorology.* Vol. 1 and Vol. 2, self published by Prof. G. C. Asnani , IITM, India, 1202 pp.

3.Jagannadha Rao, V. V. M., M. Venkat Ratnam, and D. Narayana Rao, 2002: Study of mean vertical motions over Gadanki (13.58N, 79.28E), a tropical station, using Indian MST radar. *Radio Sci.,*

4.V.V. M. Jagannadha rao, D.Narayana rao, M. Venkat ratnam, K. Mohan, and S. Vijaya Bhaskara rao Mean Vertical Velocities Measured by Indian MST Radar and Comparison with Indirectly Computed Values, JAM, April 2003.

5.Reiter, 1961, “Jet Stream Meteorology”. University of Chicago Press, Chicago, USA, 515 pp.

6.Fukao, S., M. F. Larsen, M. D. Yamanaka, H. Furukawa, T. Tsuda, and S. Kato, 1991: Observations of a reversal in long-term average vertical velocities near the Jet stream wind maximum. *Mon.Wea. Rev.,* **119,** 1479–1489.

Observing and analysing meso-scale vortices by weather radar

Zhu Xiaoyan and Xue Qiufang

State Key Laboratory of Severe Weather, Chinese Academy of Meteorological Sciences

Abstract

This paper presents a simple method for estimating the divergence and vorticity of the meso-scale vortices occurred in the Beijing-Tianjin-Hebei area based on the radial velocity data from a single Doppler weather radar. The results show that the formation of severe meso-scale weather systems is closely related to the turning or convergence/divergence in the wind field. The cyclonic vorticity should be an indicator for heavy rains, which is potentially a very powerful tool for the convection recognition.

Key words: Meso-scale vortex; Velocity image; vorticity

RADAR TRACKING METHOD FOR CLOUD SEEDING EXPERIMENTAL UNITS OVER CUBA

Sadiel Novo[1], Daniel Martinez[1], Carlos A. Perez[1], Boris Koloskov[2], Felix Gamboa[1]

[1] *Institute of Meteorology, La Habana CP 11700, Cuba, sadiel.novo@insmet.cu*
2 Agency of Atmospheric Technologies (ATTECH, ROSHYDROMET)
Novovagankovsky per. 8, Moscow, 123242, Russia, attech@mail.ru

I. INTRODUCTION

During October 2006, the second phase of the Randomized Convective Cold Cloud Seeding Experiment in Extense Areas (in Spanish, EXPerimento aleatorizado de siembra de nubes convectivas en AReas EXtensas, EXPAREX) was undertaken over Camaguey, in the eastern part of Cuba (Martinez et al, 2007). One of the main goals of this phase of the experiment was obtaining well defined experimental units for evaluating the seeding effect. In this respect, an experimental unit is defined as the clouds inside a circle of radius 25 km, centered at the location of initial seeding at the first instant, which moved along with the seeded system and inside which all the suitable clouds whose top regions were seeded (or not) with AgI ejectable flares are located. The tracking method used to follow the evolution of these experimental units, also known as floating targets, is the main objective of this paper.

II. DATA AND ALGORITHM

Basic data consisted in MRL-5 (10 cm) automated radar products obtained with software Vesta (Pérez et al., 1999; Peña et al., 2000). Two-dimensional maps of maximum reflectivity, rainfall rate at 3 km height, maximum top height and height of maximum reflectivity within a circle of radius 180 km centered in radar, were ingested every 5 min by the tracking software with the aim of calculating the coordinates of the center of the experimental unit as well as its main characteristics. Resolution of maps was chosen to be 1.5 km. Besides that, coordinates of the initial treatment point were needed to initialize the tracking.

The tracking algorithm is based on the following hypothesis: the experimental unit will follow the average movement of the surrounding storms. For each maximum reflectivity radar image, the method identifies as storms all the groups of pixels with reflectivity and area values greater than certain thresholds. The reflectivity threshold value (25 dBZ) is applied first, and consequently, connected components (up to second nearest neighbors) are labeled. Afterwards, the area threshold (7 km^2) is applied to discard the smaller echoes. Then, every echo region (storm) is associated with an ellipse, the normalized second order moments of which are equal to the ones of the echo region. This constraint leads to an eigenvalue problem allowing obtaining the parameters of the ellipse.

At the treatment instant, which is taken as initial time for tracking, all present storms are identified, and the corresponding ellipses are defined by the algorithm. The experimental unit boundary circumference is displayed, centered at the treatment point and extending to a radius of 25 km. In the next scan, every storm in the radar's field of vision is tracked by choosing the new center positions that are located at the minimum distances from the centers in the previous scan, provided a certain limit distance is not attained (typically 5 km for a time lag of 5 min between scans). After all the storms have been identified in the new step, their displacement vectors are obtained. An average displacement vector of the storms contained inside a radius of up to 100 km neighborhood of the treated cloud is then calculated. This average displacement vector is assigned to the experimental unit. As output of the processing program, an image with the last maximum reflectivity map and the subsequent positions of the superimposed experimental unit circle is obtained (FIG. 1), and also a text file including date, time, coordinates of the center and the main parameters of the seeding circle for every instant, as well as for the total tracking time. The algorithm stops to follow an experimental unit when the elapsed time with maximum rainfall rate less than 2 mm/h inside the seeding circle reaches 30 min.

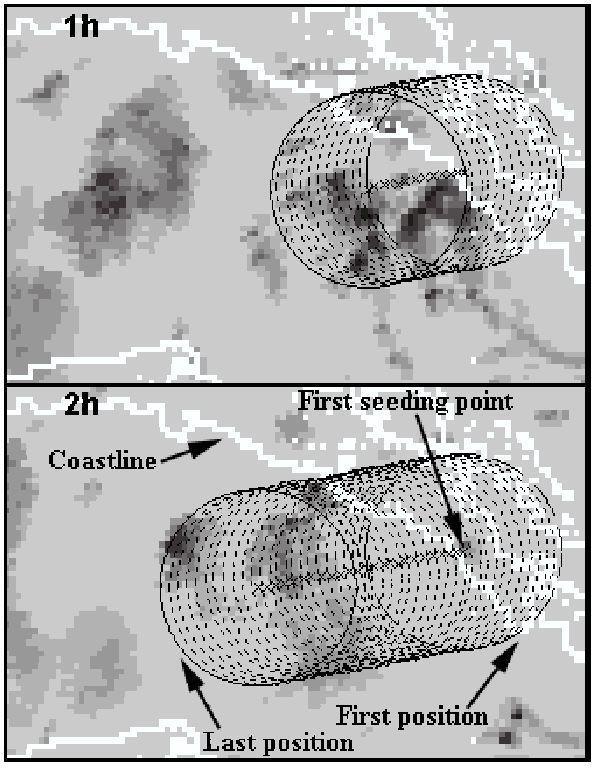

FIG. 1: Trajectory of first experimental unit for 1 and 2 h of being tracked.

III. RESULTS AND CONCLUSIONS

The tracking method was applied to the seven experimental units obtained during the second phase of EXPAREX, in which experimental flights were carried out from October 3 to October 14. TABLE I shows some tracking parameters for all of them. Date-Time stands for the date (ddmmyy) and time (hh:mm) of first seeding, TT is the total tracking time, V the mean velocity and W is the total volume of precipitation (3 km height) accumulated in the floating target during its lifetime. A plot of TT versus Log(W) for the seven 2006 experimental units is shown in FIG. 2 with circles. Notice that we do not know which ones of these seven experimental units were really seeded, because of the randomized and blind nature of the experiment.

#	Date - Time	TT (min)	V (km/h)	W (kT)
1	031006-14:20	240	27	55273
2	061006-15:20	400	11	12841
3	101006-13:50	60	12	16
4	101006-14:50	290	10	1141
5	111006-14:50	350	11	1450
6	121006-14:45	115	15	35
7	141006-15:15	525	18	25391

TABLE I: Tracking parameters for 2006 experimental units.

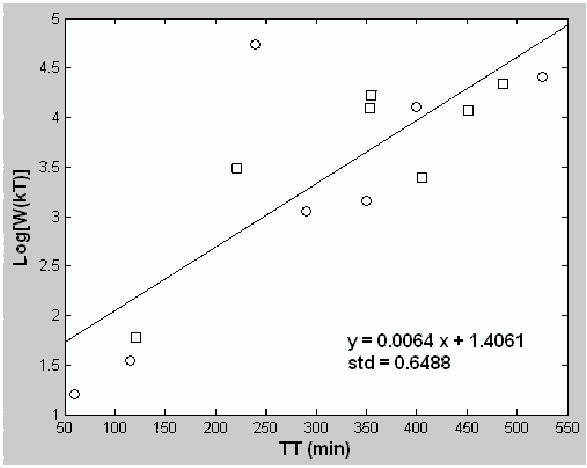

FIG. 2: Plot of TT versus Log(W) for all the experimental units in 2006 (circles) and 2005 (squares).

#	Date - Time	TT (min)	V (km/h)	W (kT)
1	030905-15:01	354	9	12446
2	160905-14:50	121	30	60
3	170905-14:52	452	25	11611
4	210905-16:19	355	12	16571
5	220905-14:30	486	17	21550
6	230905-14:46	405	15	2481
7	270905-13:53	221	10	3033

TABLE II: Tracking parameters for 2005 experimental units.

Square marks in FIG. 2 belong to data from seven experimental units more, all of them seeded, which were obtained during the first stage of EXPAREX (exploratory, non randomized experiment) in September 2005. Some tracking parameters for these 2005 experimental units appear in TABLE II. Data were adjusted linearly and the corresponding equation and standard deviation were written on the plot. From the plot we can see that there is a gap without points between 120 and 220 minutes in x axis and between 1.8 and 3 in y axis. This seems to indicate that the three cases in the lower-left corner of the graph might belong to a different statistical ensemble in relation to the rest of the sample. The 2005 case is seeded, and the treatment of the two 2006 cases is not yet known. This may be an effect of the still limited size of the sample or may be caused by specific synoptic or mesoscale situation in these cases, or may be simply a problem of wrong experimental unit selection which has to be taken care of in the future, evaluating the possibility of considering these cases as outliers. As the randomized experiment goes on, the statistical properties of the ensemble of experimental cases will become clear.

A method for tracking cloud seeding floating experimental units over Cuba has been developed. The algorithm uses maximum reflectivity maps to identify storms in the radar's field of scanning. Looking for the nearest storm's positions in the next scan, it follows the movement of each one. Then the average movement of surrounding storms is assigned to the experimental area and its parameters calculated.

With data from 14 experimental units, it was found an exponential relationship between the total precipitation volume accumulated at 3 km height and the total duration for each area. A gap without experimental units was found in the graph around 1000 kT in rainfall volume and 3 hours in duration. Points below this gap could indicate outliers, which should be clarified in subsequent analysis as the sample increases.

Radar-rain gauge calibration will give us the way to compare ground precipitation with the tracking parameters for a better evaluation.

IV. AKNOWLEDGMENTS

The authors would like to thank to the Cuban Government and particularly to the Institute for Civil Aeronautics for coordinating and financing EXPAREX.

V. REFERENCES

Martinez D., Perez C.A., Koloskov B., Korneev V.P., Petrov V.V., Gamboa F., Novo S., 2007: Randomized Convective Cold Cloud Seeding Experiment in Extended Areas over Cuba. *Proceedings of 9th WMO Conference on Weather Modificationc, October 22-24, Istambul, Turkey*

Peña A., Rodriguez O., Perez M., Naranjo R., Fernandez L., Barreiras A., Martinez A., Rodriguez M.D., 2000. Modernization of the Cuban Weather Radar Network. *Phys. Chem. Earth (B)* 25, #10-12, 1169-1171.

Perez M., A. Peña and O. Rodriguez, 1999: Reengineering MRL-5 for the Cuban Weather Radar Network. *29th International Conference on Radar Meteorology*, Montreal, Quebec, Canada, 811-814.

Simulations of X-band thunderstorms radar observations

Pujol O.[1], N. Bon[2], C. Costes[3], H. Sauvageot[4], J.P. Artis[5]
[1] *Laboratoire d'Aérologie, Université Paul Sabatier, Toulouse, France, pujo@aero.obs-mip.fr*
[2] *Thalès Systèmes Aéroportés, Brest, France, nicolas.bon@fr.thalesgroup.com*
[3] *Thalès Systèmes Aéroportés, Brest, France, clémentine.costes@fr.thalesgroup.com*
[4] *Laboratoire d'Aérologie, Université Paul Sabatier, Toulouse, France, sauh@aero.obs-mip.fr and*
[5] *Thalès Systèmes Aéroportés, Brest, France, jean-paul.artis@fr.thalesgroup.com*
(Dated: Thursday April 26th 2007)

I. INTRODUCTION

Thunderstorms are the most dangerous convective systems of the atmosphere. Their very large vertical extension and their extreme intensity in terms of precipitation are a serious problem for civil aviation. In tropical latitude, organization of several thunderstorms in mesoscale convective systems like squall lines is also of a great interest for pilots. To quantify the hazard and avoid such extreme precipitating systems, X-Band airborne radar are currently used. However, this frequency domain (f = 10 GHz, $\lambda \approx 3.2$ cm is problematic due to attenuation. It is thus important to know what a radar would really see and consequently indicate to pilots.

In this paper, we present a static model of thunderstorms to simulate the observations of an airborne X Band radar. The modeled thunderstorms are first summarized and then various features of the radar observations in X Band are discussed. Final section indicates further scientific directions.

II. MODELING OF A THUNDERSTORM

The present model is an extension to ice phases of the model used by Pujol et al. (2007a, b) to study liquid clouds. Thunderstorms contain all types of hydrometeors : ice crystals, snow and large aggregates as graupel, hail, supercooled water, rain and cloud droplets. In our model, each of these kinds of particles are characterized by a two dimensional physical variable $X(x, z)$, where x is an horizontal variable and z the vertical one, and a hydrometeor size distribution. X is chosen to be water content M (in g m^{-3}) for non precipitating particles (ice crystals and cloud droplets) and precipitation rate R (in mm h^{-1}) for the other hydrometeors. Geometrically, the modeled thunderstorm are symmetric with respect to its vertical axis; one can write $X(x, z) = X_z(z)G(x)$ where $X_z(z)$ is the vertical profile of X at the centre of the modeled thunderstorm and $G(x) = \exp(x^2/L^2)$ represents the horizontal dependence of X - at a given altitude z_i, $X = X_z(z_i)G(x)$ - with L the horizontal extension of the modeled thunderstorm. Hydrometeors microphysical characteristics is chosen to be a gamma modified distribution:

$$N(D) = N_0 D^{\mu} \exp(-\Lambda D) \qquad (1)$$

	D_{min}	D_{max}	ρ (g cm^{-3})
Ice crystal	0.1	2	0.9
Snow	1	5	< 0.2
Graupel	0.5	5	0.2-0.8
Hail	5	50	> 0.8
Rain	0.5	5	1
Cloud droplet	1	50	1

TABLE I: Various physical characteristics of the different particles considered in this study. First and second columns are the minimum and maximum diameters (in mm) of the hydrometeor size distributions; for the last line, diameters are given in μm. Third column is the density, which is necessary for computation of refractive index and then for radar reflectivity and attenuation (see following section).

where D is the equivalent diameter from 5 mm to 5 cm and N_0, μ, and Λ are three parameters which can be determined using X or other physical variable. For example, for hail, which is the most dangerous precipitation, $\mu = 0$, and (Cheng and English 1983, Sauvageot 1992):

$$N_0 = 115\Lambda^{3.63} \quad \text{and} \quad \Lambda = \ln(88/R)/3.45 \qquad (2)$$

with R in mm h^{-1}, N_0 in m^{-3} mm^{-1}, and Λ in mm^{-1}. First and second column of Table I summarizes the minimum D_{min} and maximum D_{max} equivalent diameters of the different kinds of particles. It is noteworthy indicates that all the values in our model are based upon observations referenced in many accepted and recognized studies (e.g. Sauvageot 1992, Pruppacher and Klett 1997).

III. SIMULATION OF RADAR OBSERVATIONS

Radar observations of the modeled thunderstorms are performed at frequencies of 3 and 10 GHz with a radial resolution of about 100 m and a beamwidth approximated at a 3dB aperture of 1°. Then, in each radar sample volume $\mathcal{V}$, the backscattering cross section σ and the attenuation (diffusion + absorption) cross section Q of each hydrometeor can be computed by means of the Mie theory, and then added and averaged over $\mathcal{V}$ to finally obtain the reflectivity Z(dBZ) and attenuation A(dB km^{-1}) fields in S and X Bands. Since the S Band is less attenuated and presents a first Mie mode for larger backscatterer diameters, the comparison between the $Z(A)$-fields

in S and X Bands should illustrate and quantify the differences and the problem of the X Band.

IV. RESULTS AND CONCLUSIONS

Two main results emerges from these simulations of radar observations of thunderstorms:

- Reflectivity field is degraded by hydrometeor attenuation in X Band. A particular point concerns attenuation by cloud droplets which is a non negligible source of attenuation although droplets are undetectable compared to the precipitating particles. This point has been already underlined and investigated by Pujol et al.(2007a) for cumulus clouds; this problem is all the more important that, contrary to precipitation, there does not exist a corrective method for cloud attenuation with a single radar.

- Hail detection is limited in X Band. Indeed, the most dangerous hailstones have diameters which are larger than the first Mie mode. In such a situation, hailstones have a radar reflectivity in X Band lower than the radar reflectivity in S Band. Thus, hailstones can be assimilated to very heavy rain which is less dangerous than a hail area. This problem is particularly important since a pilot would then underestimate the hazard of the region where he conducts its plane and many people.

Although simple, but reasonable and realistic, our model indicates clearly that hail detection is problematic in X Band. Either many effort are required to improve hail detection or X Band should be avoided and advantageously replaced by S Band radar.

V. FURTHER WORKS

This works suggest other ones. First, it appears necessary to propose an efficient method for hail detection if X Band continues to be used for civil aviation. Second, organization of thunderstorms in squall lines or other mesoscale convective systems should be studied. These tropical precipitating systems, which are of an extreme intensity in terms of convection and precipitation are of considerable importance for pilots. Finally, our model should not stay in a static mode and a time component seems to us necessary to take into account lifecycles of one or many convective cells. The authors are conscious that the study presented here is theoretical and need some real data for validation.

VI. REFERENCES

Cheng L. and English M., 1983: A relationship between hailstone concentration and size. *J. Atmos. Sci.*, 40, 204 - 213.

Pruppacher H. and Klett J.D., 1997: Microphysics of clouds and precipitation. Kluwer Academic Publisher 943 pp.

Pujol O., Féral L., Sauvageot H., and Georgis J.F., 2007a: Degradation of radar reflectivity by cloud attenuation at microwave frequency. *J. Atmos. Oceanic Technol.*, 24, 640 - 657

Pujol O., Sauvageot H., and Georgis J.F., 2007b: Influence of drizzle on *Z-M* relationships in warm clouds. *Atmos. Res.*, in press.

Sauvageot H., 1992: Radar Meteorology, Artech House, 366pp.

An Evaluation of ECMWF Analyses Sounding Parameters in Thunderstorm and Severe Local Storm Forecasting for Europe.

Rudolf Kaltenböck [1] and Nikolai Dotzek [2]

[1] *Austrocontrol, Aviation Weather Service, Vienna – Austria, rudolf.kaltenboeck@austrocontrol.at*

[2] *DLR -IPA, Oberpfaffenhofen - Germany, nikolai.dotzek@dlr.de*

(Dated: April 26, 2007)

I. INTRODUCTION

This study describes the environmental atmospheric characteristics in the vicinity of local severe storms in Europe during 2006 and 2007. Parameters of nearby radiosoundings were analysed to classify thunderstorms into none, weak and severe events.

II. PRESENTATION OF RESEARCH

Severe weather events from the European Severe Weather report Database ESWD (http://eswd.eu) were used to get information about different types of convective severe weather: damaging winds > 25 m/s, tornados and funnel clouds, large hail > 2 cm and heavy precipitation.

Additionally, we focused on significant tornados (F2 or more) to obtain severe events without large reporting biases. A selection of cases excludes coastal and maritime effects.

High resolution ECMWF Analyses from the T799 model were used, which are available for 2006 and 2007. The operational datasets from ECMWF cover Europe with spatial grid resolution of about 25km, temporal intervals of 3 hours and 91 vertical levels. This aspect allows us to create close pseudo proximity soundings to investigate environmental conditions associated with severe thunderstorms.

The use of high-resolution data sets takes into consideration, that in Europe local influences, e. g. from orography, are predominant. For example, in Austria a typical value of the relative storm helicity (0-3km) for severe convective events is approximately 85 m^2/s^2 accompanied by moderate CAPE. This value is low in comparison with significant severe environmental conditions in the US central plains.

Lightning data were analysed to distinguish and classify thunderstorm activity on a European scale into three categories: none, weak and strong.

These data were compared to the ESWD data and ECMWF data, from which proximity sounding parameters are calculated: low level and deep shear, CAPE, instability index, LCL height and cloud top information .

USING C-BAND RADAR DIFFERENTIAL PHASE MEASUREMENTS FOR EXTREME RAINFALL ESTIMATION: COMPARISON WITH ESTIMATES BASED ON HORIZONTAL REFLECTIVITY

R. Bechini[1], F. Zanon[2], M. Borga[2], V. Campana[1], R. Cremonini[1]

[1]*Arpa Piemonte – Area Previsione e Monitoraggio Ambientale, Torino, Italy, r.bechini@arpa.piemonte.it*
[2]*Dipartimento Territorio e Sistemi Agro-Forestali, Università di Padova, Via dell'Università, 16, Legnaro (PD), Italy, marco.borga@unipd.it*

I. ABSTRACT

Polarimetric radar capabilities are increasingly spreading from research to operational systems. Arpa Piemonte manages two polarimetric radar in North-Western Italy: Bric della Croce and Monte Settepani. This work focuses on the analysis of two flash flood events occurred during the summer of 2006. Rainfall rate at the ground is estimated by using KDP, the range derivative of the differential phase ΦDP. The accuracy of these estimates is evaluated by using raingauge measurements as a reference. KDP- based estimates are compared with concurrent estimates based on horizontal reflectivity measurements and processed by applying correction of partial beam blocking, attenuation and vertical profile of reflectivity. This comparative study aims at assessing the reliability of rainfall estimates from polarimetric measurements and quantifying the benefit deriving from the operational use of differential phase measurements for hydrological applications.